Spring 2015

Machining as a mechanical property test revisited

David L. Smith
Purdue University

Graduate School Form 30
(Revised 08/14)

PURDUE UNIVERSITY
GRADUATE SCHOOL
Thesis/Dissertation Acceptance

This is to certify that the thesis/dissertation prepared

By David L. Smith

Entitled
MACHINING AS A MECHANICAL PROPERTY TEST REVISITED

For the degree of Master of Science in Industrial Engineering

Is approved by the final examining committee:

Srinivasan Chandrasekar

Kevin Trumble

W. Dale Compton

To the best of my knowledge and as understood by the student in the Thesis/Dissertation Agreement, Publication Delay, and Certification/Disclaimer (Graduate School Form 32), this thesis/dissertation adheres to the provisions of Purdue University's "Policy on Integrity in Research" and the use of copyrighted material.

Srinivasan Chandrasekar

Approved by Major Professor(s): _____

_____

Approved by: Abhijit Deshmukh 03/04/2015

Head of the Department Graduate Program Date

MACHINING AS A MECHANICAL PROPERTY TEST REVISITED

A Thesis

Submitted to the Faculty

of

Purdue University

by

David L. Smith

In Partial Fulfillment of the

Requirements for the Degree

of

Master of Science in Industrial Engineering

May 2015

Purdue University

West Lafayette, Indiana

For my wife, Arielle

ACKNOWLEDGEMENTS

I would like to thank my friends, colleagues and mentors who made this achievement possible. Special thanks are due to Prof. S. Chandrasekar for his invaluable guidance, insight, and enormous patience throughout my work at Purdue. I would also like to thank my many colleagues: Yang, Dinakar, Anirban, Ho, and Koushik for their help when critical questions were in need of answering. Special thanks to Wayne Ewbank, for his words of encouragement and practical teaching, both the shop and in life beyond. Most of all, thanks be to my parents, for all of their support, and my wife, Arielle, whose understanding and perseverance through this time were often greater than my own.

TABLE OF CONTENTS

Page

LIST OF FIGURES

Figure Page

ABSTRACT

Smith, David L. MSIE, Purdue University, May 2015. Machining as a Mechanical Property Test Revisited. Major Professor: Srinivasan Chandrasekar.

There is much need for data on mechanical behavior of metals at high strains and strain rates. This need is dictated by modeling of processes like forming and machining, wherein the material in the deformation zone is subjected to severe deformation conditions atypical of conventional material property tests such as tension and torsion. Accurate flow stress data is an essential input for robust prediction of process outputs. Similar requirements arise from applications in high speed ballistic penetration and design of materials for armor. Since the deformation zone in cutting of metals is characterized by unique and extreme combinations of strain, strain rate and temperature, an opportunity exists for using plane-strain cutting as a mechanical property test for measuring flow properties of metals.

The feasibility of using plane-strain cutting to measure flow properties of metals is revisited in the light of recent data showing controllability of the deformation conditions in chip formation by systematic variation of process input parameters. A method is outlined as to how the deformation conditions can be varied by changing the process parameters. The method is applied to cutting of commercially pure copper (FCC),

iron (BCC) and zinc (HCP). Forces and chip geometries are measured, in conjunction with particle image velocimetry characterization of the deformation using high speed image sequences. The flow stresses are estimated from these measurements.

The measured flow stress and its dependence on strain are shown to agree well with prior measurements of these parameters using conventional tests, and flow stress inferred from hardness characterization. The method is also demonstrated to be able to measure properties of metals that recrystallize at room temperature (zinc), wherein quasi-static tests predict much lower strength. Sources of variability and uncertainty in the application of this measurement technique are discussed. Future work in the context of further evaluation of this measurement approach is proposed.

1 INTRODUCTION

Machining is widely used in the production of components to desired tolerances and geometric specifications. Indeed it is one of the most common forms of subtractive manufacturing. The extensive studies of machining have revealed a dimension to the chip formation process that suggests opportunities for its use in determining mechanical properties of metals under extreme deformation conditions. This dimension pertains to the unique and, potentially, controllable combination of strains, strain rates and temperatures that can be effected in the machining zone by varying the input process parameters such as cutting speed and tool rake angle. Concurrently, measurement of forces and deformation zone geometry in continuous chip formation enable the shear (flow) stress in the deformation process to be estimated to first order. In this estimation of the flow stress, the assumption of the deformation zone being idealized as a shear plane is necessary. By combining the deformation parameters and flow stress data it would thus be feasible to obtain the flow stress as a function of deformation parameters. This type of approach to obtaining the mechanical response of metals from chip formation measurements was suggested as early as the 1940s [1] but not fully developed.

The need for material properties at extreme deformation conditions is dictated by requirements for such data as inputs in modeling of various metalworking processes such

as rolling, drawing and machining. Such material property data is also required for analyzing/evaluating material behavior in ballistic impact and armor applications. While an abundance of tests exist for the purpose of quantifying the mechanical strengths of materials in various modes of deformation, they have some limitations. The ubiquitous tension/compression test, fundamental to most mechanical testing, is limited to flow stress data estimation at small strain rates and low-to-moderate strains. Various forms of impact tests have been developed for obtaining high strain rate behavior of metals. Table 1.1 provides a list of some of the main methods in this category, along with applicable ranges of strains and strain rates. Most of these require specialized equipment and infrastructure that are expensive. When examined against these tests, machining stands out in two respects. First, the range of strains and strain rates accessible by machining is quite large and also complements the capabilities of the other tests. Second, the infrastructure needed for using machining may be much simpler.

With this as the background, the present work seeks to explore the possible use of machining as a method for characterizing the flow behavior of metals. In a sense, it is a revisiting of the idea as exploratory attempts have been described in earlier studies [2-5]. Some of the newer aspects of the present study in this regard pertain to improved characterization of the deformation conditions underlying chip formation, better measurement capability for forces, and demarcation of the limitations of the approach.

Table 1.1: Available methods of high strain-strain rate mechanical testing

Testing Method	**Loading**	**Effective Strain**	**Effective Strain Rate**	**Notes**
Hopkinson bar impact	Tension, Compression	Up to 50%	10^2-10^4	Elastic-plastic wave propagation. Inertia forces important. Plane stress.
Hopkinson (Kolsky) bar	Shear	Up to 50%	10^2-10^4	
Taylor Impact Test	Compression	50-150%	10^4-10^5	
Expanded Ring	Tension	Up to 10%	10^4	Strain rate not constant across thickness.
Flyer Plate	Tension	Up to 25%	$>10^5$	Shock wave propagation. Inertia forces important. Plane Strain
Pressure-shear plate impact	Shear	Up to 50%	10^4-10^7	Specimen is very thin. Material must be fine-grained to study polycrystalline behavior.
Machining	**Combined**	**50-1000%**	**10-10^5**	**Large plastic deformation. Plane strain. Temperatures between ambient and melting. Strain gradient can be controlled.**

Problem Statement: Machining as a material property test for obtaining flow stress data is evaluated using plane-strain orthogonal cutting as a model deformation system. This experimental configuration is selected for relative ease of controllability and characterization of the deformation conditions, and measurement of forces. The deformation conditions and shear plane area are obtained from measurements of the deformation zone geometry and/or using Particle Image Velocimetry (PIV) analysis of high-speed images of the deformation. The flow stress is estimated from the forces, measured by a piezo-electric dynamometer, and the shear plane area. Comparisons are made with flow stress data obtained from other tests. The bulk of the tests are done at only small strain rates ($\sim 10^2\ s^{-1}$) but large strains, and the test data compared with those from quasi static tests. The validity of the approach is evaluated both with the comparison to the prior data and with controllability of deformation conditions. A discussion of the limitations and uncertainties in this method of testing are discussed both with regard to small and large strain rate testing.

The structure of this thesis is as follows. Chapter 2 reviews the mechanics of machining and the model used in this study. Chapter 3 presents prior work related to material testing and the use of machining as a test method. In Chapter 4, the experimental plan, configuration of the testing apparatus and procedures for calculation are detailed. Chapter 5 presents the results from the 2-D cutting tests. Chapter 6 discusses limitations and uncertainties involved with the current method. The conclusions drawn from these tests are discussed in Chapter 7.

2 MECHANICS OF MACHINING

This chapter reviews the mechanics of plane strain machining. An overview of machining and the constitutive equations of the process relevant to this study are presented.

2.1 Machining and Chip Formation

Machining in its broadest definition usually refers to the act of removing material from a workpiece with a sharp, wedge-shaped tool until final net shape is reached. It is the most used form of subtractive manufacturing, in which material removal is the primary production method. Many forms of machining exist each differentiated by the process parameters, geometry of the material removed, materials used, or otherwise.

All machining, however, involves the removal of material usually in the form of a thin chip. This chip is produced by the force exerted by the tool on the work material through a process involving severe shear stress and strain. If plane strain machining is considered, then the deformation zone underlying chip formation is usually thin and may be assumed to be a plane. Termed the "shear plane," this area represents a concentration of strain rate in the material. The material flowing through this zone experiences rapid shearing with the associated strain rates at high cutting speeds being often many orders of magnitude higher than those seen in quasi-static material tests. Usually the strain rate has a linear dependence on this speed. Figure 2.1 illustrates the principal feature of chip

formation in 2-D machining, which involves shear across a plan. It is a micrograph of an OFHC copper sample taken using a ‘quick-stop’ technique, where the cutting process is stopped while in progress. Visible grains in the bulk of the sample quickly become indistinguishable after passing through a thin region into the chip. Concurrently, there is a significant increase in the material hardness which is shown in the Vickers Hardness numbers superimposed onto the figure. This thin region of deformation, running from the tool tip (right) to the free surface on the back side of the chip (left), is identified with the shear plane. In this description, the flow stress during deformation can be obtained by dividing the shear force along the shear plane by the shear plane area. The shear force may be obtained from force measurements and resolving the resultant force along the shear plane. One would then have a basis for measuring the shear flow stress of the material at the appropriate strain and strain rate prevailing in the deformation zone.

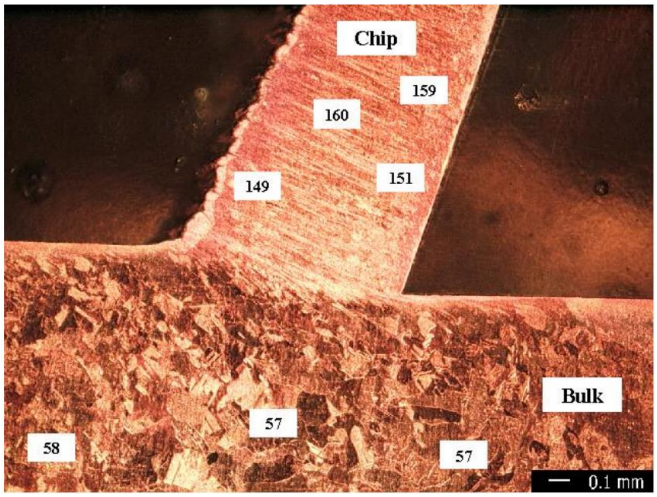

Figure 2.1: Quick-stop of chip formation in OFHC copper. The confinement of the shearing process in chip formation to a narrow zone or plane is clearly shown by the sudden change from visible grains in the bulk to the indistinguishable structure in the chip. Hardness values are superimposed on the bulk and chip, in HV (kg/mm^2). Figure from Brown [6]

2.2 Plane Strain Machining

This study will make use of orthogonal plane strain machining as the experimental configuration. This is the act of machining using a tool with a straight edge perpendicular to the direction of cutting that leaves a new surface parallel to the original material's surface and where all deformation is confined to a plane perpendicular to the cutting edge. In Fig. 2.1, as one such example, all deformation has been confined to the plane of the figure. This configuration is also unique in the fact that the resulting force system imposed on the tool and the workpiece is two dimensional, and contained in this plane perpendicular to the cutting edge.

The research done by Merchant [7, 8] and his contemporaries has provided good characterization of the continuous chip-formation deformation process in 2-D cutting, including kinematics, velocity relationships and forces. Figure 2.2 shows the shear plane model for continuous chip formation. Material is fed to the right while the tool is held stationary. In this model, the interaction of the material and tool is determined by three main process parameters: 1) rake angle, α, of the tool, 2) undeformed chip thickness, t_o, 3) cutting velocity, V_o. The first two parameters define the geometric interaction during cutting with the strain being determined by the chip thickness ratio $r = t_o/t_c$, while the velocity affects the rate of this interaction (strain rate) and the temperature in the deformation zone.

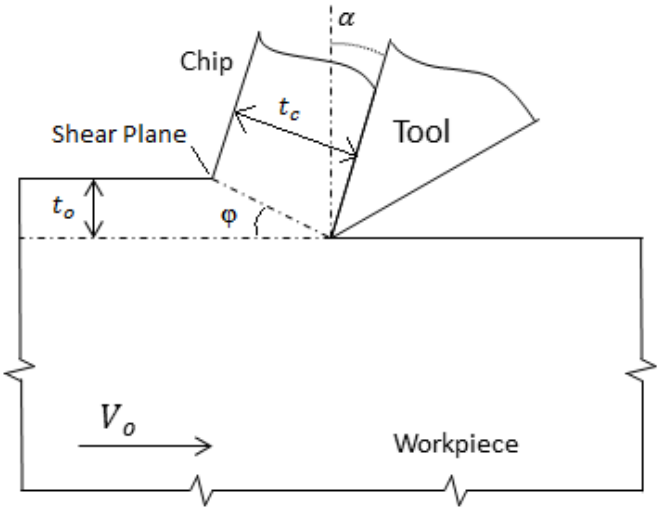

Figure 2.2: Schematic of shear plane model in machining

It is important to note that the shear plane angle, φ, measured from the cutting direction, is not prescribed, and is instead a materials response to the cutting parameters. This angle plays a large role in the calculation of the shear strain in the chip, and is found by Merchant [7] in the following sequence:

$$r = \frac{t_0}{t_c} = \frac{L_2}{L_1} \tag{1}$$

$$\tan(\varphi) = \frac{r\cos\alpha}{1 - r\sin(\alpha)} \tag{2}$$

where t_0 and t_c are the undeformed and deformed chip thicknesses, respectively, and L_1 and L_2 are the lengths of the chips before and after cutting, respectively. Merchant used these chip length measurements in place of thickness measurements under the assumption of incompressibility of the material (true for plastic deformation) and therefore constant volume before and after the cut, as well as the unchanged width of the chip. The shear strain, γ, is then obtained as:

$$\gamma = \cot(\varphi) + \tan(\varphi - \alpha) = \frac{r}{\cos(\alpha)} + \frac{1}{r\cos(\alpha)} - 2\tan(\alpha) \tag{3}$$

This equation is applicable under the condition where the shear zone is approximated as a plane, the chip is continuous, and the chip strain is homogeneously distributed without any strain localization etc.

It is clear from Eq. 3 that the shear strain can be obtained from a measurement of r and α. A first order estimate of the strain rate can be obtained as the quotient of the shear strain and the time elapsed through the shear zone. If the thickness of the deformation zone does not change with V_o, then the strain rate is seen to increase linearly with V_o providing a basis for experimentally varying the strain rate. By using a 'quick-stop' technique to freeze the machining process, images like Fig. 2.1 allow estimation of the shear zone's thickness, δ. To experimentally estimate the shear strain rate, one would only need to know the time taken to shear the material in this shear zone. Using the average of workpiece and chip velocities as an estimate of the speed through the shear zone, V:

$$V = \frac{V_o + V_c}{2} \tag{4}$$

$$r = \frac{t_o}{t_c} = \frac{V_c}{V_o} \rightarrow V = \frac{(r+1)V_o}{2} \tag{5}$$

Thus the time through the shear zone, Δt, and shear strain rate, $\dot{\gamma}$, can be estimated as:

$$\Delta t = \frac{\delta}{V} \tag{6}$$

$$\dot{\gamma} = \frac{\gamma}{\Delta t} = \frac{\gamma(r+1)V}{2\delta} \tag{7}$$

From these quantities, we have the basis for calculating the shear strain, strain rate and shear flow stress of the metal during cutting. Thus by recording straightforward measurements, it should be possible to extract stress and strain data of a material at

various strains and strain rates using plane strain orthogonal cutting as a test method. Alternatively, the strain and strain rate may be obtained from PIV analysis of high speed images of the material flow [9].

Merchant also provided an understanding of the forces involved in the cutting process as pictured in Fig. 2.3. This is simply the result of the total force acting on the tool, R, being resolved into components in various directions of interest; three pairs are shown. These components are as follows: 1) F_c, the force in the cutting direction and F_t the (thrust) force perpendicular to the newly produced surface, 2) F_s, the component of R along the shear plane and F_n, the R component normal to the shear plane, and 3) F, the frictional force along the tool rake face and N, the force normal to the rake face. It is the norm to express the various force components in terms of the measured forces; these are usually F_t and F_c.

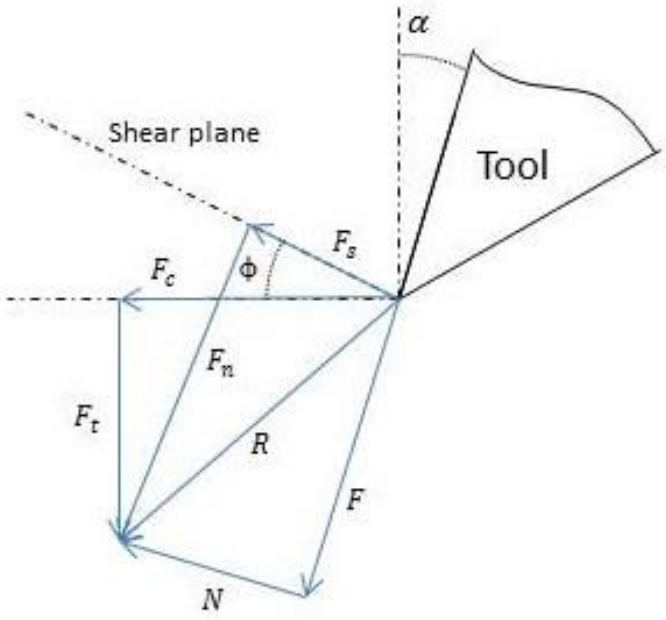

Figure 2.3: Forces in shear plane model of orthogonal machining

The shear force, F_s, is the force relevant to estimating the flow stress. From the force diagram, this is shear force obtained as:

$$F_s = F_c \cos\varphi - F_t \sin\varphi \tag{8}$$

The area of the shear plane, A_s, can be found from chip thickness measurements, which then permits the calculation of the shear flow stress of the material, τ:

$$A_s = \frac{A_o}{\sin\varphi} = \frac{wt_0}{\sin\varphi} \tag{9}$$

$$\tau = \frac{F_s}{A_s} = \frac{\left(F_c \sin\varphi \cos\varphi - F_t \sin^2\varphi\right)}{A_0} \tag{10}$$

where A_o is the cross sectional area of the material to be cut perpendicular to the cutting direction and w is the width of the cut. The corresponding set of equations for effective stress, strain rate and strain are as follows, which are the analog of uniaxial test parameters and allow for data comparison:

$$\bar{\sigma}_{\text{tension}} = \sqrt{3}\,\tau_{\max} \tag{11}$$

$$\bar{\epsilon}_{\text{tension}} = \frac{\gamma_{\max}}{\sqrt{3}} \tag{12}$$

$$\dot{\bar{\epsilon}}_{\text{tension}} = \frac{\dot{\gamma}_{\max}}{\sqrt{3}} \tag{13}$$

Through equations used by Efe et al. [10] and others before [11], a simple estimation of the temperature on the shear plane during cutting can also be made. The specific shear energy of chip formation is presented as:

$$u_s = \frac{2F_c}{3\,(t_o w)} \tag{14}$$

Equation 14 is based on the fact that approximately 2/3 of the energy of chip formation dissipates at the shear plane [12]. Some of this dissipated energy is absorbed as heat on the shear plane, and some flows into the workpiece. The heat absorbed by the workpiece

can be represented by the parameter Γ, which depends on many physical attributes of the material (density, ρ, specific heat, c, thermal conductivity, k) and process parameters (V_o, t_o, α). The form of Γ can be written as:

$$\Gamma = \frac{1}{4Y}(\mathrm{erf}\sqrt{Y}) + (1+Y)\mathrm{erfc}\sqrt{Y} - \frac{e^{-Y}}{\sqrt{\pi}}\left(\frac{1}{2\sqrt{Y}} + \sqrt{Y}\right) \tag{15}$$

where:

$$Y = \frac{R\tan(\varphi)}{4} \tag{16}$$

$$R = \frac{\rho c V_o t_o}{k} \tag{17}$$

$$\varphi = \tan^{-1}\left(\frac{r\cos\alpha}{1 - r\sin\alpha}\right) \tag{18}$$

Using the above formulation, one can compute an estimate for the temperature on the shear plane, T:

$$T = \frac{(1-\Gamma)u_s}{\rho c} + T_{amb} \tag{19}$$

where T_{amb} is the ambient temperature of the cut material. The dependence of Γ on V_o plays a large role in the determination of the temperature of the shear plane. At high speeds, this temperature can increase drastically due to adiabatic heating of the shear zone, whereas at low speeds temperatures can be only slightly above ambient due to rapid conduction of this heat away from the shear zone. Supplementary control of this shear zone temperature can also be accomplished by heating or cooling the material before cutting.

In summary, techniques have been developed to allow the control of strain, strain rate, and temperature through the proper manipulation of process parameters. The rake

angle can be altered to change the strain in the chip during cutting. Strain rate and temperature of the shear zone can be influenced through careful selection of the cutting speed and material temperature. These variables form the basis of controls desired for using machining as a mechanical property test. These controls combined with the high strain and strain rate capabilities of machining are what make machining such an attractive method for the measure of flow stresses under these conditions.

3 PRIOR WORK IN MECHANICAL TESTING

Some common test methods and prior work in the realm of high strain and high strain rate testing is reviewed here. This also includes the use of machining in similar studies to the present work, where measurement of material behavior was the goal.

3.1 High Strain Testing

One of the most common high strain tests used today is the compression test. In this test a cylindrical sample is compressed between two parallel platens while force and displacement are recorded. While this typically provides stress results in strains much higher than that found in the simple tension test, problems arise due to barreling, which complicates the testing. The strain rates are also quite small (~10^{-4}-10^{-3} s^{-1}).

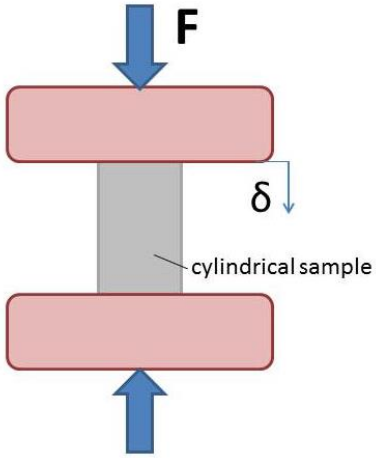

Figure 3.1: Basic compression test

It is known that under large hydrostatic compressive stresses and elevated temperatures, tension tests can be extended to much higher strains than at standard temperature and pressure conditions. The work of Bridgman [13] displayed this for a number of materials. Under these conditions, materials showed much higher strain at fracture. Here even tungsten (brittle), which fractures in tension at atmospheric pressure

at strain of ~ 0.2 failed at strains greater than 1.5 at the highest tested pressures. All the materials tested, including single crystals and brittle amorphous materials experienced ductile strain under high hydrostatic pressures. It is however quite difficult to carry out tension tests under superimposed hydrostatic pressure due to the cumbersome equipment required. Bridgman also used axial compression to extend the ductility of ductile metals tested in torsion [14]. Using hollow tubes with two notches around the circumference, the shear strain from torsion is contained to two regions, where the rod is simultaneously subjected to compression along the axis. In 1045 and 1.25C Steel, marked increases in shear strain at fracture were observed. Shear strains of 2-3 were observed at the largest compressive loads, approaching that seen in machining. Both of Bridgman's studies here show promise in the high strain regions, but cannot access phenomena seen when testing at high speeds, such as strain rate and temperature effects.

The work of Lindholm et al. [15] actually comes much closer to the mechanical conditions of machining, but still falls short in strain rate. Again using torsion to test OFHC copper samples, extreme ductility was observed to the point where all samples surpassed shear strain of 6 without fracture. While their test method was able to reliably produce flow stress data at strain rates of about 300 s^{-1}; these are much smaller than the maximum rates realizable in machining. Johnson et al. [16] continued this work applying it to several different metals of differing crystal structures. Similar torsion tests were used on OFHC copper, cartridge brass, nickel 200 (FCC), Armco IF iron, carpenter electrical iron, and 1006 steel (BCC). Shear stress and shear strain data were collected for the six materials at strain rates varying from quasi-static to greater than 300 s^{-1}. The quasi-static tests demonstrated similar behavior to traditional low strain tests such as positive strain

and strain-rate hardening. At higher strain rates, thermal softening was present causing less strain hardening in the materials due to near adiabatic heating of the gage sections. A reduction in average fracture strain was seen at higher strain rates, while localized strains due to thermally induced instabilities greatly exceeded the average. This severe localization of strain was seen in both of the above works and approaches what is seen in the typical metal shearing process during machining. In order to produce a continuous chip as used in this study, no fracture can occur in the shear zone while the chip material is subjected to large strains. These studies capture that fact which gives some validity to comparing their results to those in cutting.

3.2 High Strain Rate Testing

Material testing at high strain rate conditions typically involves the use of high speed testing equipment and measurement techniques. All mechanical property tests occupy different domains with respect to effective strain and strain rate in the sample tested. Figure 3.2, building on Table 1.1, is a bubble chart of common tests used for high strain rates.

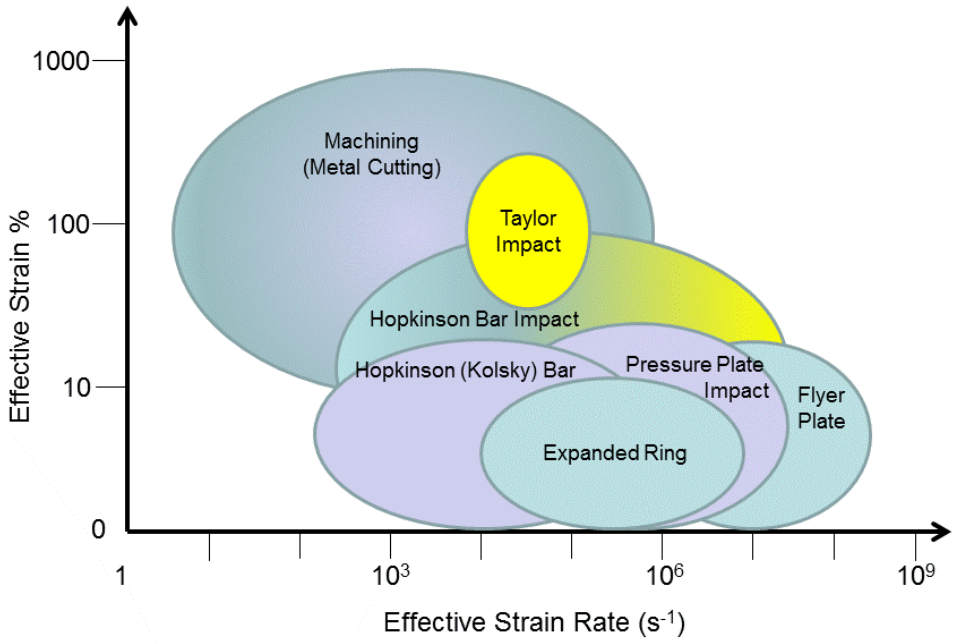

Figure 3.2: Test methods for high strain rates

One of the common tests is the split Hopkinson pressure bar (impact) test. Typically in this test, a small short cylindrical specimen is compressed at high speeds between the ends of two rods. A pressure pulse launches a striker bar into the incident bar, thereby impacting the sample against the end of the transmitter bar. The impulse wave strength and speed is measured by the strain gages. Using this information the plastic work done on the sample can be calculated as the energy lost in the wave's transmission while the strain in the sample can be measured. With a few reasonable assumptions, the flow stress behavior of materials can be measured at high strain rates on the order of several thousand per second [17, 18].

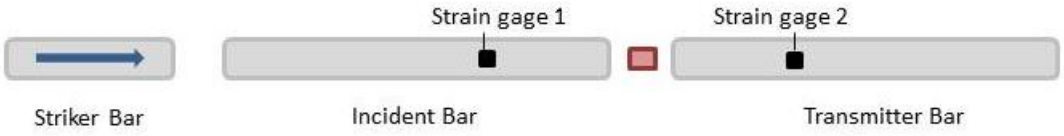

Figure 3.3: Schematic of split Hopkinson pressure bar test

This method was used by Lindholm and Yeakley [19] to obtain stress-strain curves in both tension and compression for 1100-0 aluminum at a few strain rates. They were able to capture the strain rate hardening of aluminum when subjected to the same strain under increasing speeds, reaching strain rates up to 2,600 s^{-1}. Although the strain rate levels possible in this type of test can match those in machining, the strain levels attained are small with effective strains typically less than 25%.

Glenn and Bradley [20] also made use of the split Hopkinson pressure bar technique to examine the strain rate sensitivity of OFHC copper at room temperature. Their specific goal was to quantify the "relative magnitudes of the dynamic contribution (particle inertia, suppression of thermal assistance, and so forth) and the non-dynamic contribution (namely, the accelerated rate of strain hardening observed at high strain rates)" to the increase in stress. The copper samples were strained at a rate of approximately 500 s^{-1} and then reloaded quasi-statically to yield. The difference between these reloaded samples and stress data taken during static tests was deemed the non-dynamic effect on the stress and was found to be about 60% of the total increase in stress. The dynamic effect was the difference between the original dynamically compressed stress data and the reloaded samples' data. In total, the dynamic stress was about 25% higher than the static stress data over the strain range of 0.08 to 0.2. This gave some insight into relating static material properties to the dynamic response observed in

machining. However, the strains and strain rates obtained, similar to those found by Lindholm and Yeakley, are not close to those typical of machining.

One of the most commonly cited works in this area is the investigation of Johnson and Cook [21]. To move away from simply adjusting model parameters until simulations matched experimental results, a series of tests were run to record constitutive properties of materials under known conditions. Therefore, twelve materials were tested with the aim of developing a model to accurately describe material behavior at elevated strains, strain rates, and temperatures. They employed the Hopkinson bar tensile test, rapid torsion test, and quasi-static tension test to supply data under these various conditions and derive the appropriate constants for their model. Tension tests were also used as a comparison to the torsion data by converting stresses through the von Mises flow rule (Eqs. 11 and 12). Shear data for all twelve materials was gathered from strain rates ranging from quasi-static to 400 s^{-1} in torsion. In all, they collected some of the most used data to date when referring to these heightened conditions of strain and strain rate in metals. To validate the developed model, cylinder impact tests were also used and showed good agreement with predicted deformations.

Alder and Phillips [22] ran compression tests on aluminum, copper, and steel in order to expand the quantitative information available for industrial rolling processes. Samples were compressed at a range of strain rates 1 to 40 s^{-1} as well as varying temperatures. Results found were typical in the way that increased stresses were found at given strains when increasing strain rate or decreasing temperature. Their work was aimed at understanding these parameters effects on the compression of the materials, however their efforts also explored the idea of expressing the flow stress in a material as

a function of strain, strain rate and temperature, an idea pioneered by Zener and Hollomon [23]. While expressions found by Alder and Phillips show agreement with their measured results, the two also recognize the unlikelihood of any reasonably simple expression agreeing with results obtained over wider strain rate and temperature ranges.

Zener and Hollomon tested alloy steel (0.25%C) in rapid tension to investigate similar effects. The tensile strengths at various strain rates and temperatures were compared at strains of 0.01. It was found that the tensile stress increase by increasing the strain rate could also be obtained by decreasing temperature, that is, an increase in strain rate was found to be equivalent to a certain decrease in temperature and vice versa. They assumed that temperature and strain rate were related through a dimensionless quantity that, like many other characteristic rates of materials (relaxation, diffusion, etc.), relies on an activation energy. This led to the concept of the Zener-Hollomon parameter, $Z = \dot{\varepsilon} e^{\frac{Q}{RT}}$, which incorporates the combined effect of temperature and strain rate into a single quantity. They hypothesized that if their concept was true, some computation instead of experimentation could be used to obtain adiabatic stress-strain relations where high temperatures were involved and difficult to measure with certainty. The Zener-Hollomon approach has become an important basis of evaluating flow stress data especially for studying temperature-strain rate effects on flow. The use of a Zener-Hollomon parameter has become an integral part of the description of flow stress data for many metals.

Several of the torsion tests also reviewed above in the previous section have much higher strain rates than could be considered as static. While results of these tests in rapid torsion hold some promise through rapid shear strain of the material, their strain rates are vastly overshadowed by traditional machining processes found in practice.

3.3 Machining as a Mechanical Test

The act of measuring shear flow stress during machining was done by Merchant [8] in 1945, and possibly earlier. Drucker explicitly suggested the use of machining as a property test for flow stress in an early paper around the same time [1]. With force measurements taken during the cutting process and chip geometry measured after the cutting, calculation of material shear flow strength is in theory possible. Merchant used length ratios of chips instead of thickness ratios in his expressions to calculate the shear plane angle, shear strain, and shear flow stress of 0.45%C alloy steel. While Merchant does not go on to compare his experimental values to other measurements (perhaps due to lack of data), this presents the first steps toward the use of machining to examine a material's strength.

The work of Chao and Bisacre [24] later in the 50's, in the course of a study of process parameter effects in machining of 0.27% C steel, estimated the flow stress using the Merchant approach. The measured data was similar to that recorded in other dynamic tests in that the flow stress was seen to increase with cutting speed (i.e., strain rate).

Experimental quantification of the strain rate seen in machining was attempted by Kececioglu [13] using a method of freezing the machining process by a 'quick-stop' in cutting. Other attempts to quantify the strain rate in machining operations include publications by Drucker [1], Freudenthal [25], and Chao and Bisacre [24]. These prior estimates of strain rate were mainly theoretical in nature and experimental measurements were widely unavailable at the time. The basic approach of Kecectiouglu was to measure the deformation zone size using metallography and estimate the time required to impose the deformation. Strain was obtained from chip thickness measurements. Based on the

strain and time of deformation, the strain rate was estimated as the ratio of the two quantities. This approach is similar to that underlying Eq. 7 in the present study. In turning of a 1015 steel tube under various V_o, α, and t_o, Kececioglu estimated strain rates from 0.4×10^4 up to 19.8×10^4 s^{-1}. These numbers, while consistent with prior theoretical estimates, had the advantage of being derived from experimental data.

Similar work was performed by Kobayashi et al. [4] on examining the shear flow stress on the shear plane. By examining only the shear force against the shear plane area over different rake angles in SAE 1112 steel, a linear relationship between the two quantities was noted. However, there was a non-zero positive intercept when the shear force corresponding to zero shear-plane area was estimated by extrapolation. Since a zero shear plane area corresponds to zero undeformed chip thickness, the force intercept should ideally be zero. Various explanations have been suggested for this discrepancy [26-28]. These include a "size effect" at small cut depths, the shear plane area being larger than calculated due to a bulging effect on the free surface before the chip, friction not accounted for on the flank face of the tool, and a so-called plowing effect due to the finite (non-zero) tip radius of the tool. Plowing refers to material displacement, as in sliding, without its actual removal as a chip. Kobayashi et al. suggested that this non-zero force intercept term be removed from the shear force prior to estimating the shear stress, so the estimated shear stress is purely associated with plastic deformation in chip formation and not including effects of plowing, friction etc. This approach is also used in the present work when estimating the shear flow stress.

Lira and Thomsen [29] also highlighted the attractive features of machining as a mechanical property test - especially, accessing strain rates as high as 10^6 per second,

effective strains greater than 2 without fracture, and seemingly possible large variations in temperature. In their tests, photographs and motion pictures were taken of samples being cut in plane strain conditions, where the samples had lines inscribed parallel to the direction of cutting. Deformation of these lines, analogous to streamlines in fluids, showed the shear zone to be not a perfect plane, but a diffuse region, as also noted by Kececioglu [30].

Ramalingam and Hazra [5] used force and chip geometry measurements in cutting to investigate mechanical properties of single crystals of 1100 aluminum. They found that even in different orientations, the (dynamic) shear stress on the macroscopic shear plane (not the individual slip planes) was constant, and independent of crystal orientation and cutting conditions. Also the shear flow stress was in good agreement with that measured for polycrystalline Al. The cutting forces and chip geometries, however, varied with the crystal orientation but the constancy of dynamic shear stress was maintained. These investigations proved that the use of machining as a test also may be useful for studying effects of texture, grain size, etc. on flow stress properties. These findings are somewhat contrary to those of Williams and Gane [2] who performed cutting experiments in several metals in both annealed and fully work-hardened conditions: copper, gold, aluminum (FCC), iron (BCC), and magnesium, zinc and titanium (HCP). They found that that the crystal orientation influenced the observed shear strength. Samples with the primary slip plane aligned with the shear plane yielded shear flow stresses sometimes 40% below those of samples with the primary slip plane oriented parallel to the cutting direction. They also proposed that the plowing effect due to non-zero tool tip radius is the likely explanation for a positive intercept when cutting force is plotted against the undeformed

chip thickness (an analog of the shear force vs. shear area used before by others). This additional force was subtracted from the measurements before flow stress calculation, as it does not contribute to the shearing process during chip formation. The flow stresses obtained from the annealed and work-hardened samples did not differ greatly from each other. This is most likely due to the large strains imposed during machining where the sample reaches strain saturation regardless of the prior state. Lastly, their measured flow stress showed good agreement with the strength predicted by hardness measurements made on the same materials (based on hardness-flow stress relation of Tabor [31]).

These works form a basis for the current endeavor. The current work seeks to use many of these established practices and procedures in conjunction with improved measurement techniques to investigate the practicality of using machining as a test for assessing flow stress of metals at large strain and strain rates.

3.4 Particle Image Velocimetry (PIV)

In situ observation of the cutting process is also used in the present work in the experiments involving pure zinc. This view of the process occurs at high spatial and temporal resolutions through the use of a high speed camera. This method is capable of directly measuring strain and strain rate in cutting, and is used here as a supplementary measurement to qualify the results seen from the cutting tests. While a very detailed description of the fundamental theory and setup of PIV is given by Guo [32], a brief description will be given here.

Particle image velocimetry (PIV) takes much of its fundamental theory from the study of particle movements in fluid flow. By tracking the movements of ensembles of particles, the displacements, velocities, and deformation fields of the flow can be measured. Applying this idea to metals in cutting, such as in this study, is possible by introducing surface asperities through abrasion and treating these as the particles flowing in the medium. As the material is subjected to the cutting experiment, high speed image sequences are taken and digitized for analysis with a program written in MATLAB. Each consecutive pair of images in the selected sequence is then analyzed through correlation techniques to yield displacement fields of the flow, with the velocity field resulting from dividing by the time interval between the two images. Spatial and temporal differentiation of these fields result in the strain and strain rate fields used to characterize the metal flow. Should the reader desire more information on PIV, please refer to Ref. [33, 34]..

4 EXPERIMENTAL

This chapter will detail the experimental setup of the present work including the configurations and important details of the linear slide used for cutting and a tension machine used for tension testing. Necessary instrumentation used for measurement is also included.

4.1 Cutting Tests

The cutting system used consisted of a linear slide with a material holding fixture and a (stationary) mounted tool in the form of a sharp wedge. By fixing the tool at a known height relative to the sample material's surface, the cut was executed by moving the material mounted on the linear slide against the tool at a desired velocity. This setup is modeled after plane strain cutting discussed in Chapter 2, and shown in Fig. 2.2.

The linear slide was actuated by a Parker Hannifin J series servo motor providing speeds of 0.1 – 200 mm/s. Control of this slide was through Motion Planner software on an attached computer. The slide was set in front of the tool mount fixture where the tool would be fixed above the sliding workpiece holder (Fig 4.1). Tools used for the cutting experiments were Thinbit® HSS wedge inserts of different wedge angles so as to allow for fixation into different rake angle positions. The tool holder was mounted on a

Kistler type 9254 three-component dynamometer to measure the cutting and thrust forces. The depth of cut, i.e., undeformed chip thickness t_o, was measured and verified by taking the difference of the sample's height before and after the cut. This was done with a Mitutoyo Height measurement stand using a dial indicator with a resolution of 2.5 µm (0.0001").

The experimental setup is shown below in Fig. 4.1 and a close-up in Fig. 4.2. Some high speed images were also taken of the cutting process in zinc to augment the measured data and give *in situ* perspective of the cutting through strain and strain rate calculation. The image sequences were analyzed using an image correlation method known as Particle Image Velocimetry (PIV). This method is detailed later in this chapter.

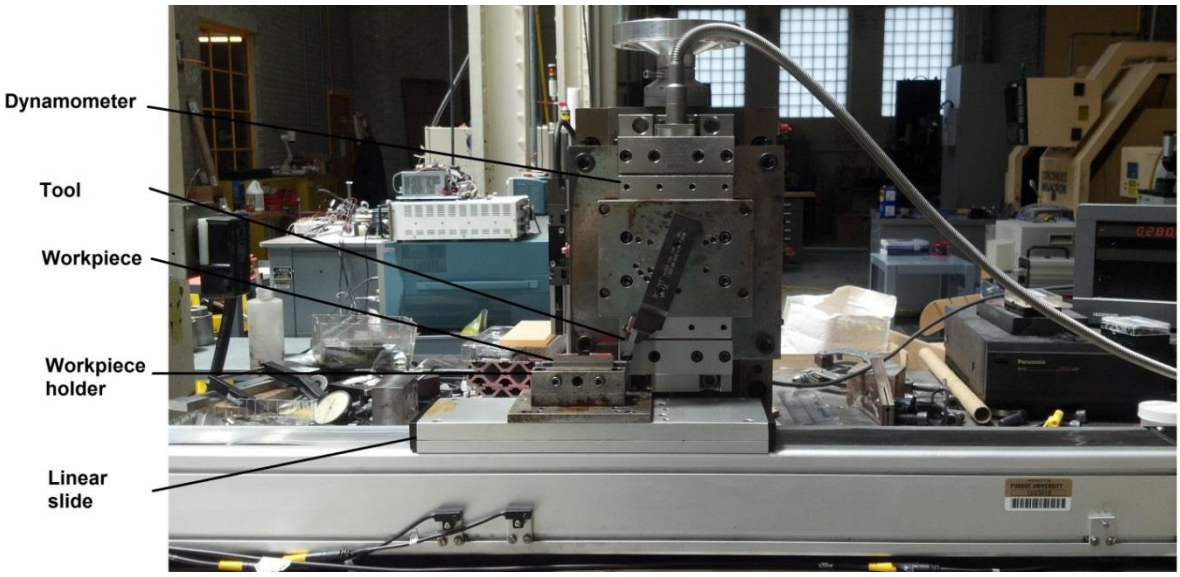

Figure 4.1: Experimental setup

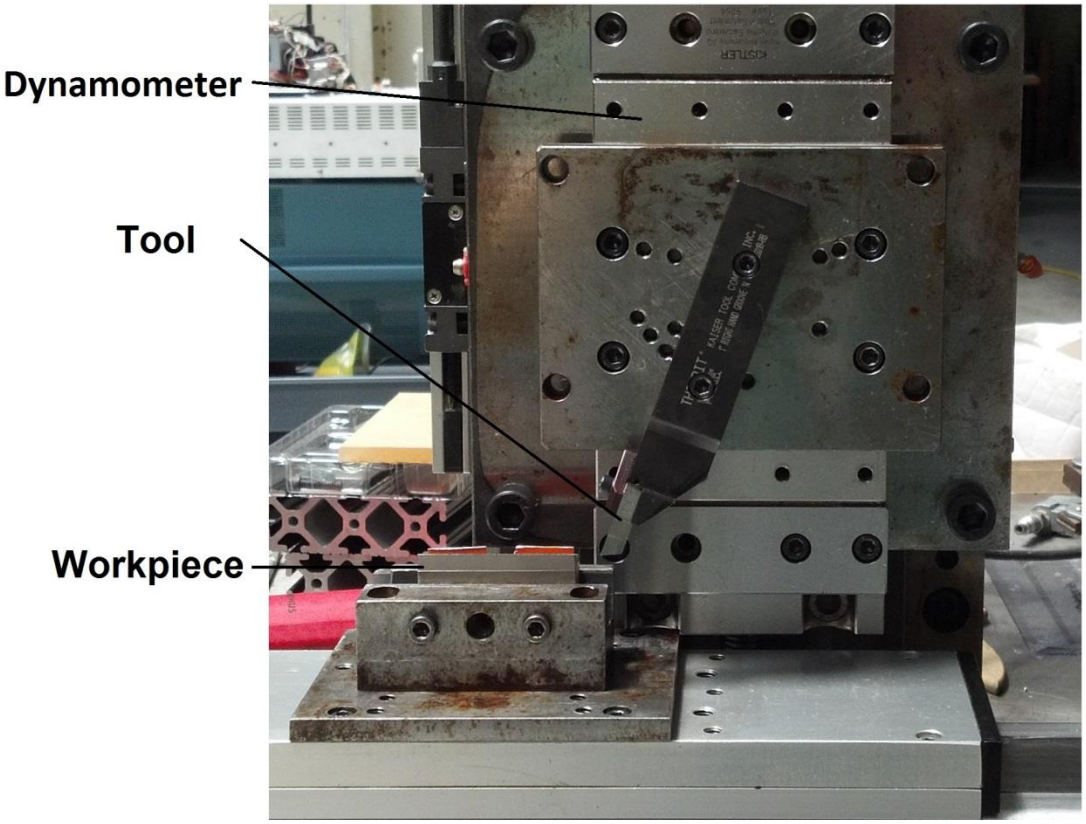

Figure 4.2: Close up of experimental setup. The tool is mounted on the dynamometer. The workpiece is mounted on the linear slide and passes under the tool to achieve material removal

4.1.1 Test Specimen

The general shape of the test specimen for the cutting is shown below in Fig. 4.3. The critical dimension of the piece is only the width w at the top where the cut occurs. This width needs to be much greater than the cut depth to promote plane strain in the chip formation; in the present experiments w was kept at over ten times t_o. Generally, w was greater than 1.5mm and t_o less than 100 μm. The workpiece materials tested were annealed OFHC Copper (C10100, 99.99%, 83HV, 50g), strain-hardened OFHC Copper (121HV, 50g), as-received pure iron (105HV, 50g), and rolled pure zinc (41HV, 50g).

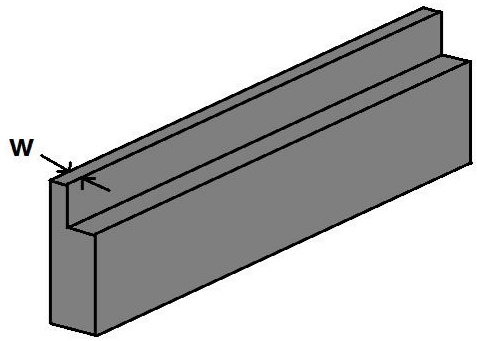

Figure 4.3: Test specimen. Material is cut during the test along the length of the specimen, at the top with cut width w

As-received OFHC copper was heated to 700°F for four hours and air cooled for use as the annealed condition. Some OFHC copper was also strain-hardened using a rolling mill, reducing the thickness by ½ so as to impose an effective strain of 0.7. The (hardened) samples for testing were cut out of the rolled strips after removing regions that underwent inhomogeneous deformation near the edges and surface.

4.1.2 Cutting Test Parameters

Several cutting conditions were used in the cutting experiments. Most samples were cut at a linear speed of 10 mm/s with t_o of 50 µm. To observe effects of strain rate on the shear flow stress, strain hardened OFHC Cu was also cut at speeds of 1 and 100 mm/s. Several strain conditions were tested for each material as well. By using α of 0°, 10°, 20°, and 30°, the strain in the chip was varied and recorded throughout the trials. Five trials were performed at each condition while recording the force data during cutting. Below is a table showing the plan of cuts for the present study.

Table 4.1: Plan of experimental cuts

Hardened Cu	α			
V_o (mm/s)	30°	20°	10°	0°
1	5 cuts each			
10				
100				

Annealed Cu, Zinc, Iron	α			
V_o (mm/s)	30°	20°	10°	0°
10	5 cuts each			

Each successive cut test is performed by resetting the fixtures and relocating the tool downward the appropriate t_o. The chip for the next test is then removed from what remains of the sample from previous cuts. However, in materials where significant strain hardening is experienced in the subsurface after machining this proves to be an issue. In the iron and annealed copper samples, for instance, care had to be taken to remove this hardened sublayer before recording the next cut. The extent of deformation in this sublayer depends on α and t_o during the cut. This effect has been examined before by Guo

[32], where it was seen that after cutting brass at $\alpha=10°$, $t_o=150$ µm, and $V_o=10$ mm/s, appreciable strain reached about 35 µm into the subsurface. In the present study, this concept was used to remove the hardened sublayer. For $\alpha=0°$, 50 µm was removed before the next cut test. At $\alpha=10°$, 20 µm was removed, and at $\alpha>10°$, the hardened sublayer was considered negligible to t_o, since imposed subsurface deformation decays so rapidly with increasing α.

4.1.3 Chip Characterization

After each cut was made, the chip was removed and collected. This chip was then mounted into epoxy-resin with the thickness of the chip being the cross-section visible to the observed surface. Chip clips were used to set the chips upright during mounting so that the true side cross section could be viewed for measurement. The mounted chip was polished with progressively smaller grit polish paper, diamond particle paste, and colloids: 600, 320, and 120 grit SiC paper, 15, 6, and 3µm diamond paste, colloidal silica and a final polish ending with colloidal alumina (<1µm particle size). The chip thickness, t_c, was measured on the cross-section through the use of an Olympus GX51 optical microscope coupled with a PC using PAX-it! imaging software. Vickers hardness measurements were taken on the mounted chips using a LM247AT LECO micro-hardness tester. Four indentations were made on each chip of each α value of each material and averaged to give a representative hardness of each cutting condition. The indentation sizes were manually measured via the microscope cross-hairs.

4.1.4 Force Measurement

By mounting the cutting tool on the dynamometer, force measurements were recorded during cutting. This is shown in Fig. 4.2, with the dynamometer component axes being aligned with the cutting and thrust force directions. Figure 4.4 below shows a sketch of the cut process with an example of a typical force-time plot.

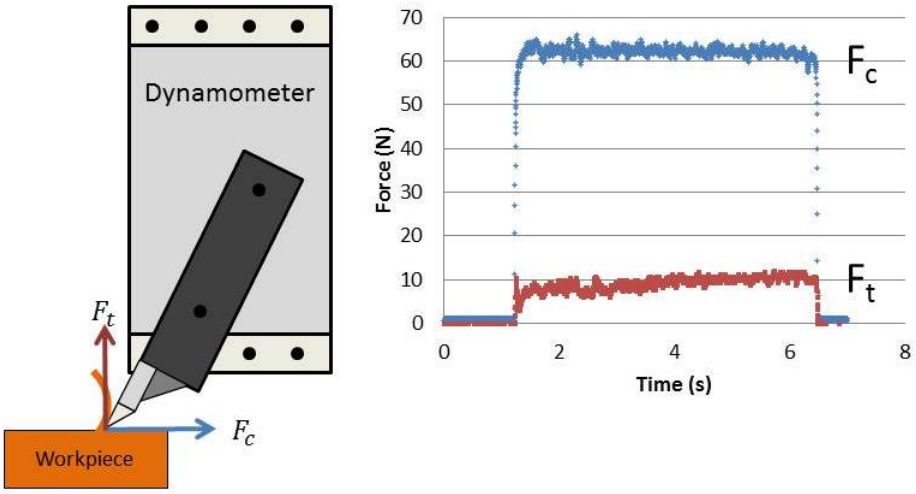

Figure 4.4: Example of cutting force data taken during cutting

From this force trace data, a simple average cutting and thrust force is calculated using only the force points in the steady state of the cut. Often, the force during the cut begins in a transient state but eventually reaches a constant value. In these cases, only the steady state region is included as the characteristic force. Note also that the chip thickness measurements were also only taken at locations corresponding to this steady state region. One such example of a force trace is shown below.

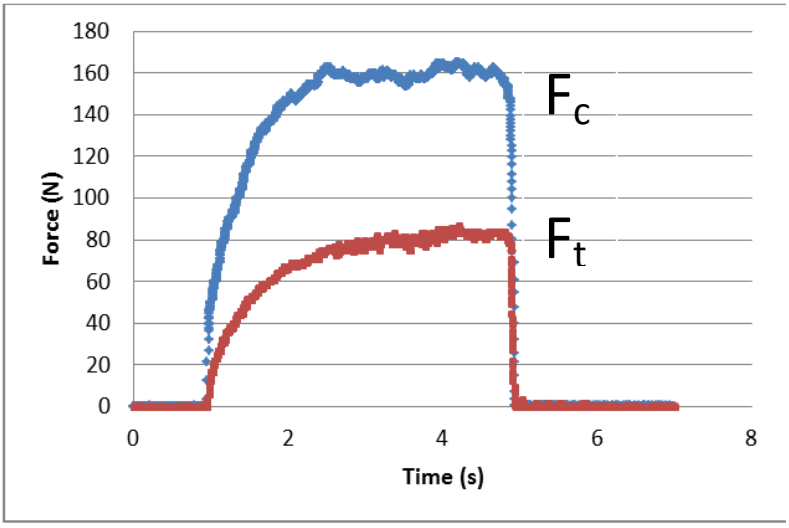

Figure 4.5: Example of transient force during orthogonal cutting. Steady state data used here for calculations would be from 3-4.5 seconds, for example

Force data was collected for each of the five trials at each α condition for each material and used in estimating the flow stress.

4.2 Calculations

The above measurements allowed the estimation of strains and flow stresses at the various deformation conditions in the tests. The strain rate is also obtained for the zinc cutting experiments from PIV image analysis. In the strain and flow stress estimation, the primary shear zone is approximated as a shear plane.

4.2.1 Strain Calculation

The shear strain on the shear plane was estimated from the measured chip thickness, t_c, and the undeformed chip thickness, t_o, using Eq. 3 in Chapter 2:

$$\gamma = \cot(\varphi) + \tan(\varphi - \alpha) = \frac{r}{\cos(\alpha)} + \frac{1}{r\cos(\alpha)} - 2\tan(\alpha) \quad (3)$$

The chip thickness ratio, r, which is dependent on the material's increase in thickness as it is sheared into the chip, is in essence a measure of the strain but not determined or set *a priori* in cutting. Hence the strain is varied by simply changing α (Eq. 3). In the application of constrained machining, r can be set *a priori* enabling greater control of the strain.

4.2.2 Methods of Shear Flow Stress Calculation

The measured force values were used to calculate the shear flow stress of the material. The shear flow stress is obtained by dividing the shear force by the area of the shear plane. Equations 2 and 8-10 in Chapter 2 were used for these calculations. Using the force data and measured chip thickness ratios, these equations allow the calculation of the shear flow stress:

$$\varphi = \tan^{-1}\left(\frac{r\cos(\alpha)}{1-r\sin(\alpha)}\right) \tag{2}$$

$$F_s = F_c\cos(\varphi) - F_t\sin(\varphi) \tag{8}$$

$$A_s = \frac{t_o * w}{\sin(\varphi)} \tag{9}$$

$$\tau = \frac{F_s}{A_s} \tag{10}$$

4.2.3 Shear Force Friction Correction

Before estimating the flow stress, the shear force data must be corrected for any finite non-zero intercept that may prevail at zero chip thickness as discussed earlier [2, 26-28]. The correction must be applied to get a true shear force to help prevent errors in the shear flow stress calculation.

To correct for the non-zero intercept in the forces at zero chip thickness, a series of cuts at each α were made with varying t_o (25, 50, and 75 µm). For each value of α, plotting the resultant force, that is, the net force combination of the cutting and thrust force, against the shear plane area allowed for identification of the force intercept at zero chip thickness. An example of one such plot is shown below as Fig. 4.6.

At a zero t_o, intuition would suggest the resultant force from cutting should reach zero as well. However, viewing the plot in Fig. 4.6, this is not the case. This non-zero intercept is taken as the force associated with the friction/plowing forces, a force needed to slide/displace the tool in the cut, but not contributing energy to shearing in chip formation.

The positive intercept force value is subtracted from the resultant force in each of the cutting experiments to get the corrected resultant force. This corrected force is then resolved onto the shear plane to get the true shear force which is then input into the shear flow stress calculation

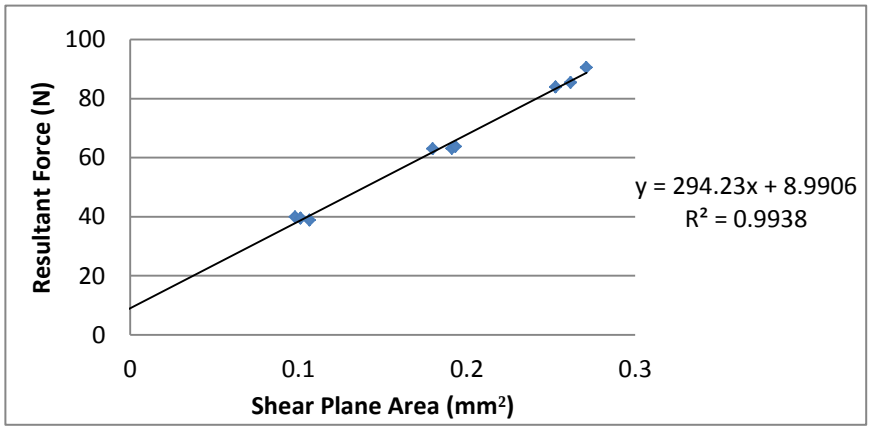

Figure 4.6: Force correction plot showing a non-zero intercept of 8.99N, the force to be subtracted from the raw cutting force data

4.3 Tension Testing

A series of tension tests was also performed on both the annealed and hardened copper and zinc. Because the cutting stress-strain data is in the high strain domain, these tension tests were conducted to acquire stress data for low strain regions using the same sample material. The pieces were pulled on an MTS QTest/50LP tension machine at a rate of 1.27 mm/min (approximate strain rate of 4.5×10^{-2} s^{-1}) until fracture. Plate style specimens were cut to ASTM E8/E8M-13a standard using the sub-size specimen dimensions, shown below in Fig. 4.7. Results including elongation, load, and time were all recorded using TestWorks software. Loads were recorded through a single axis MTS dynamometer (part no. 4501033) with a maximum load of 50 kN. Figure 4.8 shows the results of the tension tests for the three materials plotted until necking.

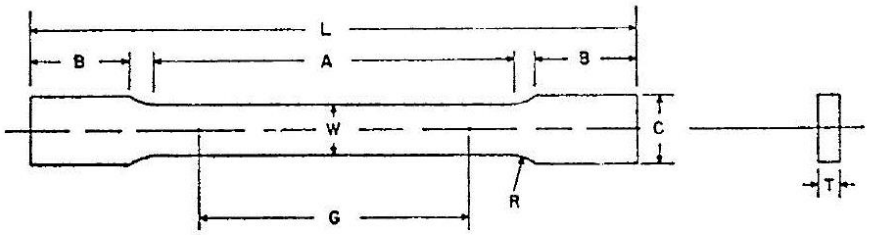

	mm
G – Gauge Length	25.0 ± 0.1
W – Width	6.0 ± 0.1
T – Thickness	thickness of material
R – Radius, min	6
L – Overall Length, min	100
A – Length of reduced section, min	32
B – Length of grip section, min	30
C – Width of grip section, approximate	10

Figure 4.7: ASTM E8/E8M-13a standard sub-size specimen dimensions for use in tensile testing with sheet type material

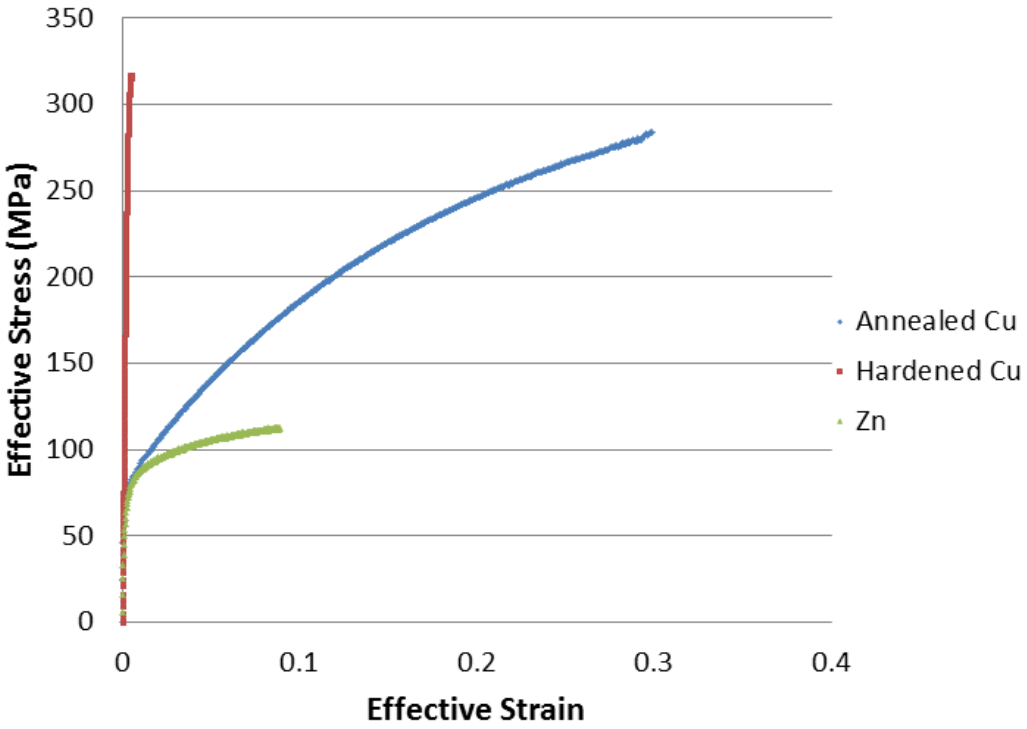

Figure 4.8: Tension test data

As can be seen in Fig. 4.8 above, very little strain was accomplished in the hardened OFHC copper tension test. This can be attributed to its pre-hardened state; these tension tests necked immediately upon yielding. This hardened state is also responsible for the initial yield point being higher than in the annealed copper specimens. The yield point of the hardened copper was about 310 MPa while both annealed copper and zinc yielded at around 75 MPa.

4.4 Particle Image Velocimetry (PIV)

The deformation field was also directly measured in a small series of experiments with cutting of zinc to obtain the strains and strain rates directly. The strains could be compared with the estimates from chip thickness measurements, and strain rates typical of the cutting test could be established. For this purpose, several sequences of high speed images were taken during the cutting. PIV analysis was used to obtain strain and strain rate fields. A schematic and photograph of the experimental setup is shown in Figs. 4.9 and 4.10 respectively.

A PCO Dimax high speed camera with Nikon Optiphot lenses was used to capture the image sequences. The field imaged was 1440 x 1100 pixels (width x height) at a spatial resolution of 1.47 μm/pix. In order to ensure a better quality in the PIV analysis, the frame rate was selected so that the movement of the sample was no more than 8 pixels between each frame (900 frames per second, at V_o= 10 mm/s). This is simply to aid in the image correlation step in the analysis, as too much material displacement between frames reduces accuracy of the image correlation. To facilitate easier viewing of the results, t_o was also increased to 125 μm.

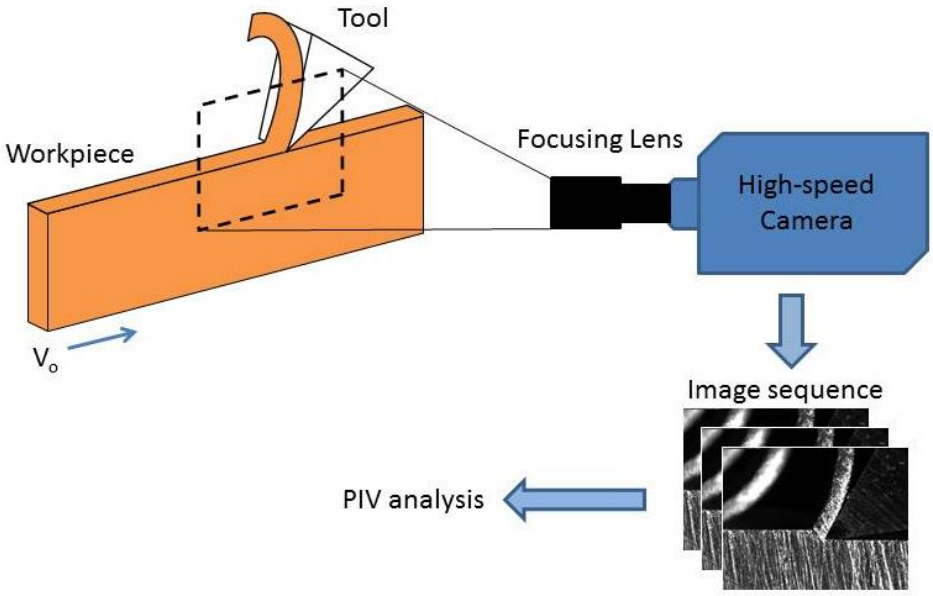

Figure 4.9: Basic schematic of PIV data acquisition. Images are taken with a high speed camera, digitized, and analyzed in a MATLAB program

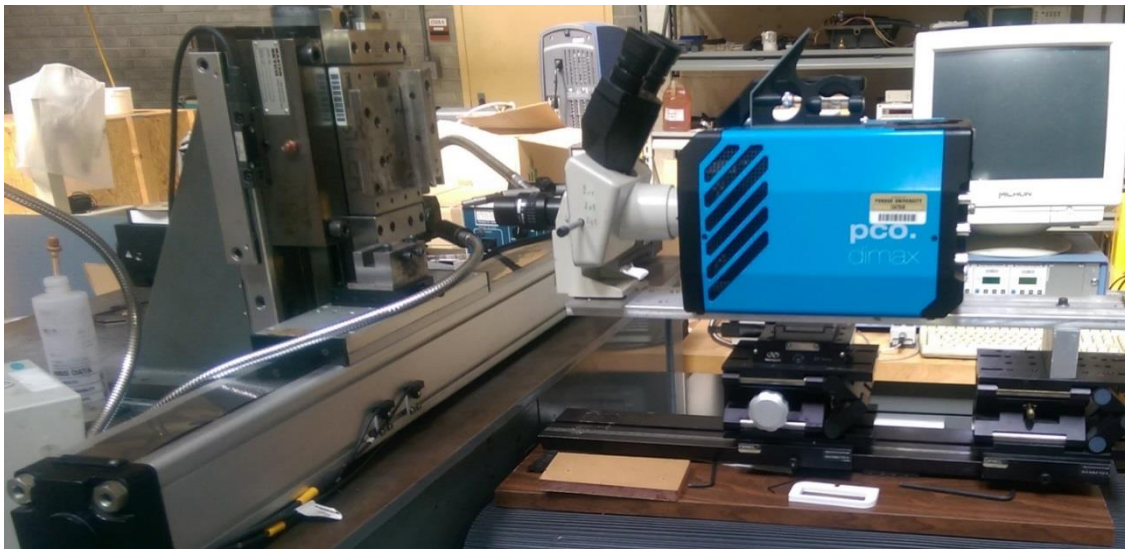

Figure 4.10: Photograph of PIV setup. High speed images are recorded by the camera viewing the cutting process from the side, that is, parallel to the cutting edge

The camera is set to record images in the plane perpendicular to the cutting edge. This records a side view of the plane strain cutting. Careful considerations of image focus and lighting are taken to ensure good image quality (contrast, brightness, etc.) for the analysis. The program used in MATLAB was developed in the manufacturing research group of S. Chandrasekar at Purdue University and was provided by Guo [9, 32].

5 RESULTS

The flow stress and strain data from the cutting experiments are presented. Materials were characterized in terms of their shear flow stress and strain imposed in the chips.

Using the horizontal linear machining set-up, a series of cutting experiments was performed on four different materials. Stress and strain data were collected for annealed OFHC Copper (C10100, 99.99%, 83HV50g), strain-hardened OFHC Copper (121HV50g), commercially pure iron (105HV50g), and pure zinc (41HV50g). The tool rake angle was varied from 0° to 30° for each material at t_o = 50 μm and V_o = 10 mm/s. The purpose was to impose different levels of strain. Pre-hardened copper was also cut at speeds of 1 and 100 mm/s to evaluate if strain rate effects could be seen in the data.

5.1 Control of Shear Strain for Testing

To access different levels of strain in the chip material during cutting, α was varied, and the strain estimated using Eq. 3 of Chapter 2. For machining, as α becomes less positive (or more negative) the shear strain in the chip increases. It is also true that as α becomes more positive (or less negative), the strain in the is chip typically reduced considerably. This can be seen in Fig. 5.1 below from data taken from all the materials in the experiments, demonstrating the control of shear strain imposed with the setting of α. The extent of

strain variation over the same range of α is different for each material, reflecting the nature of the deformation particular to each material. For both states of copper, a shear strain range of about 7 was realized. This range was γ = 3.5-10.5 in the annealed copper, and γ = 2 to 9 in the hardened copper. Iron and zinc showed much smaller ranges of strain. In zinc, the shear strain varied only from 2 to 3.5, while in iron it was between 6 and 8.5.This behavior is important, as it determines the range of strain over which flow stress data can be obtained.

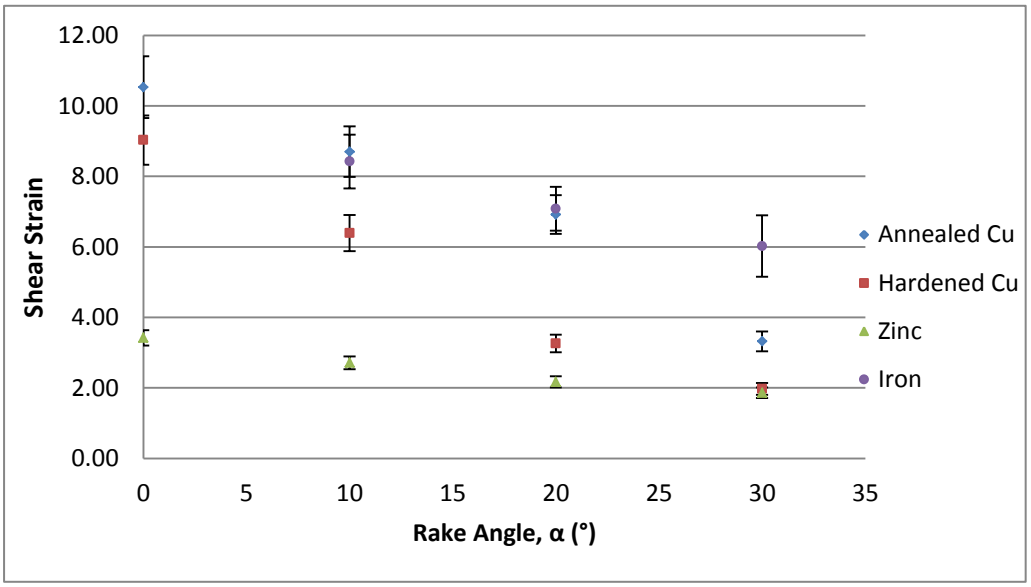

Figure 5.1: Variation of shear strain with rake angle. V_o=10 mm/s, t_o=50 μm

5.2 PIV Strain and Strain Rate Results

Figures 5.2 a-d show the effective strain rate field in cutting of zinc as the rake angle is reduced from 30° to 0° in steps of 10° (PIV measurements were made only in zinc in the present study). The region of intense strain rate may be identified with the deformation zone. It is evident from the figure that the deformation zone is quite confined, spread over a region only ~50 μm thick, and that this zone can therefore be idealized as a shear plane

for the purpose of flow stress estimation. This provides justification for the shear plane approximation even for an HCP metal. Prior work using PIV analysis has shown a similarly confined shear zone in FCC metals like copper [32]. Thus the shear plane approximation of the deformation may be justified for a spectrum of metals.

The average strain rate in the deformation zone is tabulated in Table 5.1. This is seen to vary between 75 ($\alpha = 30°$) and 150/s ($\alpha = 0°$) with the higher strain rates occurring at the smaller rake angles. Since the cutting speed was constant (10 mm/s) in this experiment, the observed variation in strain rate is likely due to the different levels of strain imposed at the different rake angles. Since the strain rate (see Eq. 7) varies typically linearly with V_o [32], the above strain rate measurements can be extrapolated to get a first order estimate of the strain rate at lower and higher speeds, for the various α.

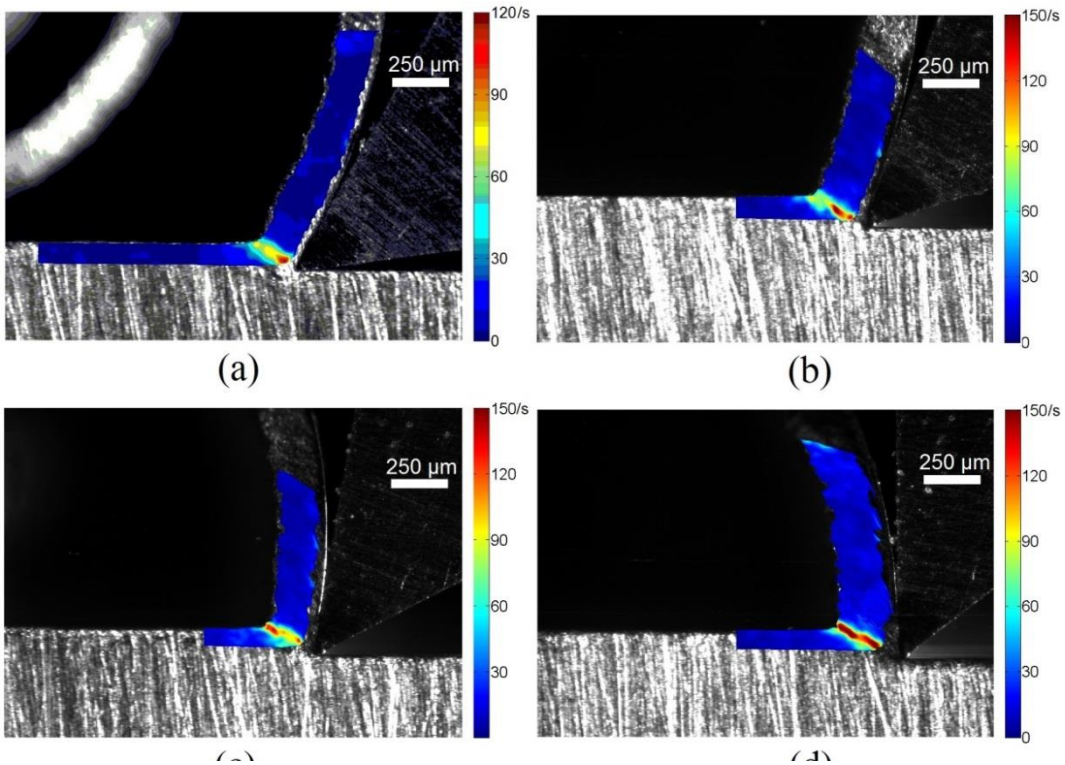

Figure 5.2: Strain rate mappings of zinc cutting. α= (a) 30°, (b) 20°, (c) 10°, (d) 0°. Vo=10mm/s, to=125 µm

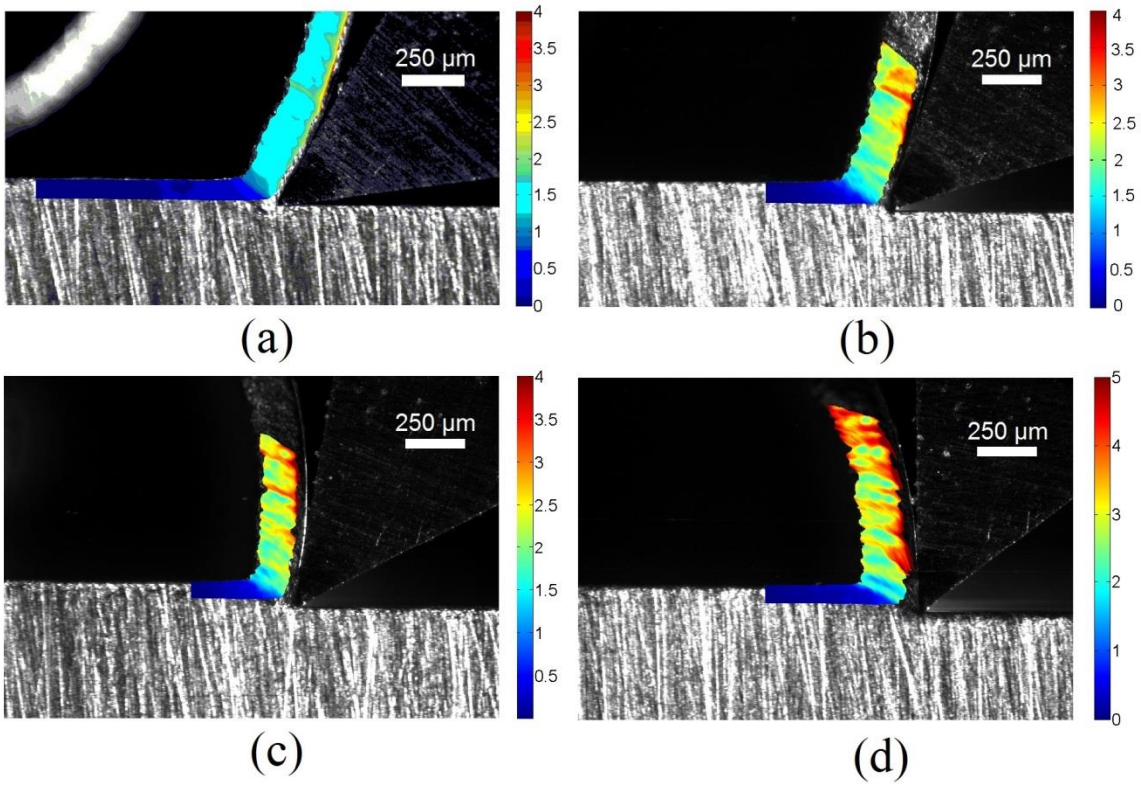

Figure 5.3: Strain fields in cutting of zinc. α= (a) 30°, (b) 20°, (c) 10°, (d) 0°. V_o =10mm/s, to=125 µm

Figures 5.3 a-d show the strain distributions in the deformation zone and chip for the various α. These fields are obtained by accumulating the strain along path lines of flow through the strain rate fields [32]. A representative strain value for the imposed strain may be obtained by volume-weighted averaging of the strain in the chip. These strain values are tabulated in Table 5.1. It is interesting to compare these strain values with the corresponding strain values derived from chip thickness measurements (also tabulated in Table 5.1). As seen from the table, the agreement between the two sets of strain values in zinc is reasonably good, varying by about 0.6 (~25% of the full range of strain). While zinc only experienced a maximum of 2.6 strain, this variance of 0.6 strain would only decrease in significance for materials such as the present copper or iron,

whose maximum effective strains were 5-6. This provides further affirmation for the use of strain values derived from chip thickness estimates as representative strains for a given flow stress.

Figure 5.3 shows that the strain distribution in the chip, while quite uniform at the larger α, becomes somewhat non-homogeneous at the smaller α. Indeed, the strain pattern has a banded appearance at the smaller α suggesting some level of localization.

Table 5.1: Results of PIV Analysis

α	Strain Rate	Strain (PIV)	Strain (measured)
30°	75	1.5	1.07
20°	100	2	1.25
10°	110	2.25	1.56
0°	150	2.6	1.98

In summary, the PIV measurements suggest the shear plane model may be used even with HCP metals and reinforces the basis of flow stress estimation by taking the shear force and dividing it by a representative shear plane area.

5.3 Flow Stress vs Strain Data

Figure 5.4 shows the variation of shear flow stress with shear strain for the four metals, as derived from the cutting measurements. Figure 5.5 averages the data groups for each material, based upon cutting conditions, to show the material's averaged behavior in the tests. The individual data points for shear and effective stresses and strains (conversion by Eqs. 11 and 12) are also tabulated in Table 5.2. Perhaps the principal conclusion that can be drawn from the figures and Table 5.2 is that the flow stress appears to have reached

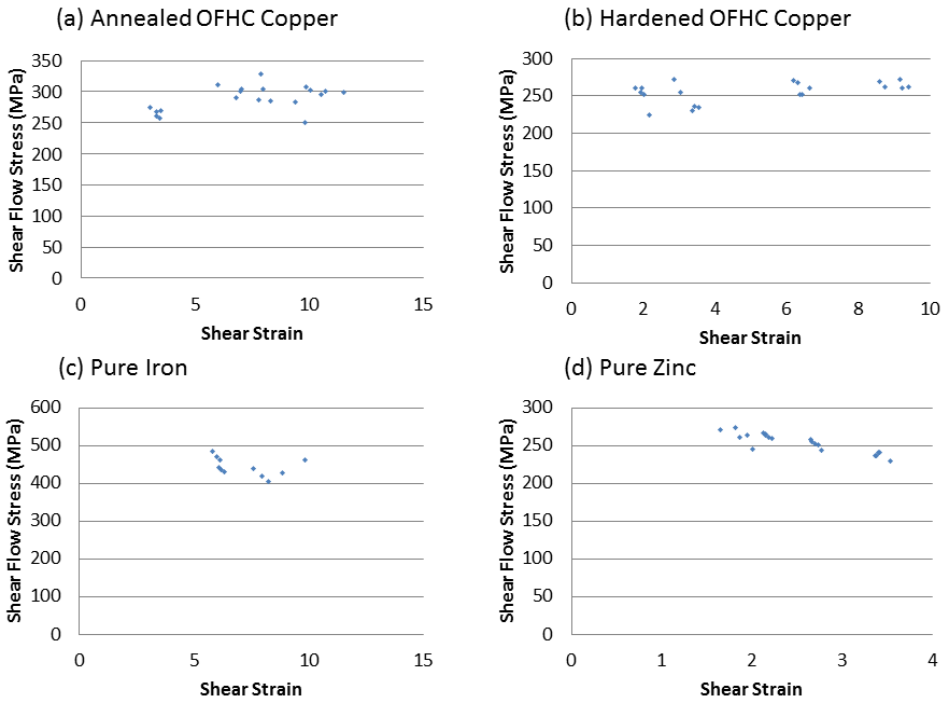

Figure 5.5: Shear flow stress vs. Shear Strain data from the cutting. V_o= 10 mm/s, α=0°-30°, t_o = 50µm

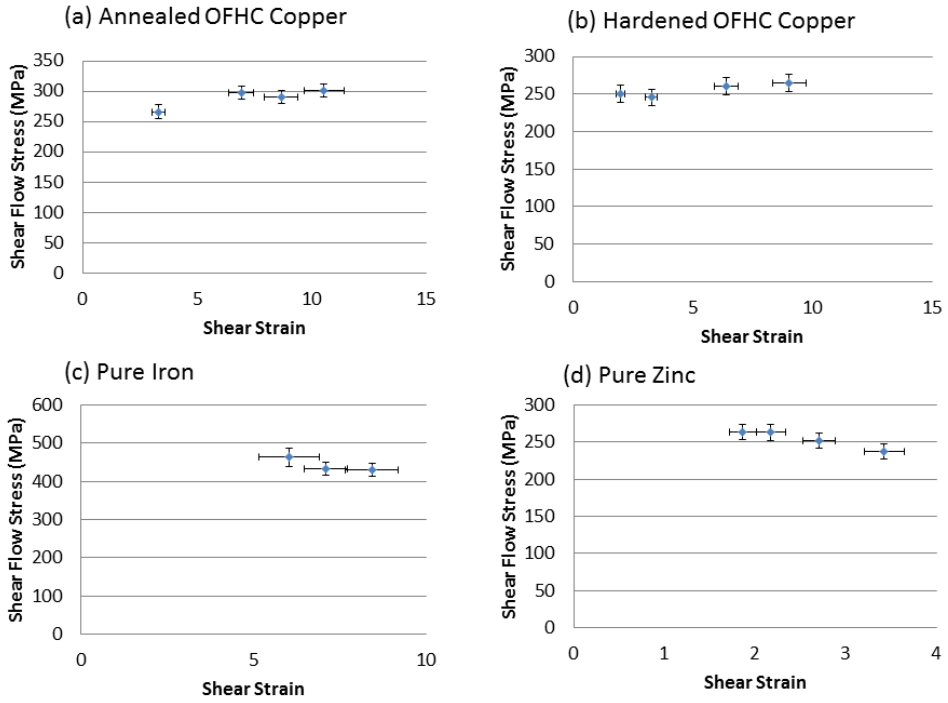

Figure 5.4: Average Shear flow stress vs. Shear strain. The averages of stress and strain were taken from 5 trials at each strain (rake angle) condition.

a saturation value even at the smallest strain. This is inferred from the negligible variation (< 10%) of flow stress with strain in the figures. A similar plateauing out of the flow stress has been noted in prior work [4, 5].

Table 5.2: Collected data for the cut materials, Stresses in MPa, V_o=10 mm/s, t_o=50 μm.

	Annealed Cu		Hardened Cu		Zinc		Iron	
α	γ	τ	γ	τ	γ	τ	γ	τ
30°	3.32	266	1.97	250	1.86	263	6.02	463
20°	6.92	298	3.26	245	2.17	263	7.08	433
10°	8.70	290	6.39	261	2.71	252	8.42	431
0°	10.53	301	9.03	265	3.42	237		
	ε	σ	ε	σ	ε	σ	ε	σ
30°	1.92	461	1.14	434	1.07	456	3.48	802
20°	4.00	516	1.88	425	1.25	456	4.09	750
10°	5.00	502	3.69	451	1.56	437	4.86	746
0°	6.08	521	5.21	459	1.98	410		

Several additional observations can be made with reference to Figs. 5.4 and 5.5. The flow stress for the copper was essentially the same for both the (initial) annealed and strain hardened samples. This is likely due to the fact that the strains imposed during the cutting were much higher than the pre-hardening strain of ~0.7, and, consequently, with both material states the saturation strain level (for flow stress) is realized during the cutting. The highest flow stress of 750 MPa, among the metals, was measured for iron. For reference, iron also has the highest yield stress among these metals in conventional tensile testing, where the as-received iron has an estimated yield strength of about 490MPa, based on bulk hardness measurements. The typical flow stress values for zinc in the cutting tests were ~440 MPa, a value that is 4 times its tensile strength in tensile testing (110 MPa). This is most likely because zinc recrystallizes readily at near

(standard) room temperatures; hence, quasi-static tests on this material often predict low strengths. In contrast, both coppers reach about 300 MPa effective stress in the tension tests, where their cutting flow stresses reach around 450-500 MPa, a ratio of about 1.5. This difference between zinc and the other materials can be explained by strain rate effects at the shear plane temperatures estimated in the following section.

5.4 Temperature of Shear Plane

Estimation of the temperature on the shear plane during cutting was done through the use of Eqs. 14-19 in Chapter 2 [10, 11]. These calculations are based on preset values of α, V_o, and t_o, and measurements of the cutting force and deformed chip thickness, as well as material constants (c, k, ρ). Table 5.3 below displays the range of temperatures for the shear plane between α of 30° and 0° (30° and 10° for iron).

Table 5.3: Shear plane temperature estimates (°C). V_o=10 mm/s, t_o=50 µm

α	Annealed Cu	Hard Cu	Hard Cu (100 mm/s)	Zinc	Iron
30°	36.2	34.8	47.0	39.8	49.2
0°	38.7	38.1	55.9	41.0	62.6 (α=10°)

Estimated from an ambient temperature of 30°, the trials of copper and zinc where V_o=10 mm/s did not vary more than a few degrees through the range of α and saw a maximum absolute temperature increase of only 11°C. The hardened copper temperatures at V_o=100 mm/s were found to be expectedly higher than its slower counterpart, having a maximum temperature of 55.9°C. Iron saw the largest overall temperature estimates at 62.6°C for α=10°. For reference, none of these temperatures represent an appreciable increase when compared to the recrystallization temperature, typically ~0.5 T_m (copper:

406°C, iron: 632°C), which is usually where larger strain rate effects begin to emerge. The only possible exception here is with zinc, where 0.5 T_m is about 74°C. The temperature predicted in cutting (and even the ambient temperature) are much closer to this 0.5 T_m in zinc, which would explain this drastic difference in flow stresses found in tension testing versus cutting.

A common expression for the flow stress as a function of strain rate is given in Hosford [35] as:

$$\sigma = C\dot{\varepsilon}^m \tag{20}$$

where C is a constant, $\dot{\varepsilon}$ is the true strain rate, and m is the strain rate sensitivity. Most materials at room temperature have near zero magnitudes of m (0 to 0.03). As a material approaches and exceeds 0.5 T_m, however, m can rise to 0.1 or 0.2, greatly increasing this sensitivity. This is likely the reason for the large increases in flow stress in zinc between the tension tests and cutting, where the strain rates vary from ~10^{-2} to ~10^{2} and the temperature is reasonably close to a homologous temperature of 0.5. By examining the ratio of the flow stresses from cutting and tension in zinc of 4, we can estimate m in these tests as:

$$\frac{\sigma_{cutting}}{\sigma_{tension}} = \left(\frac{\dot{\varepsilon}_{cutting}}{\dot{\varepsilon}_{tension}}\right)^m \Rightarrow 4 = \left(\frac{10^2}{10^{-2}}\right)^m$$

where m is calculated as around 0.15, indeed large enough to produce significant strain rate effects in the recorded data of flow stresses between cutting and tension.

5.5 Strain Rate Effect on Flow Stress

A preliminary study of the effect of strain rate on flow stress was also done with hardened copper. For this purpose, the strain rate was varied over ~ 2 orders of magnitude by varying V_o between 1 and 100 mm/s. Five trials were performed at each condition. As before, shear flow stress and shear strain were calculated and plotted. Figure 5.6 summarizes the data.

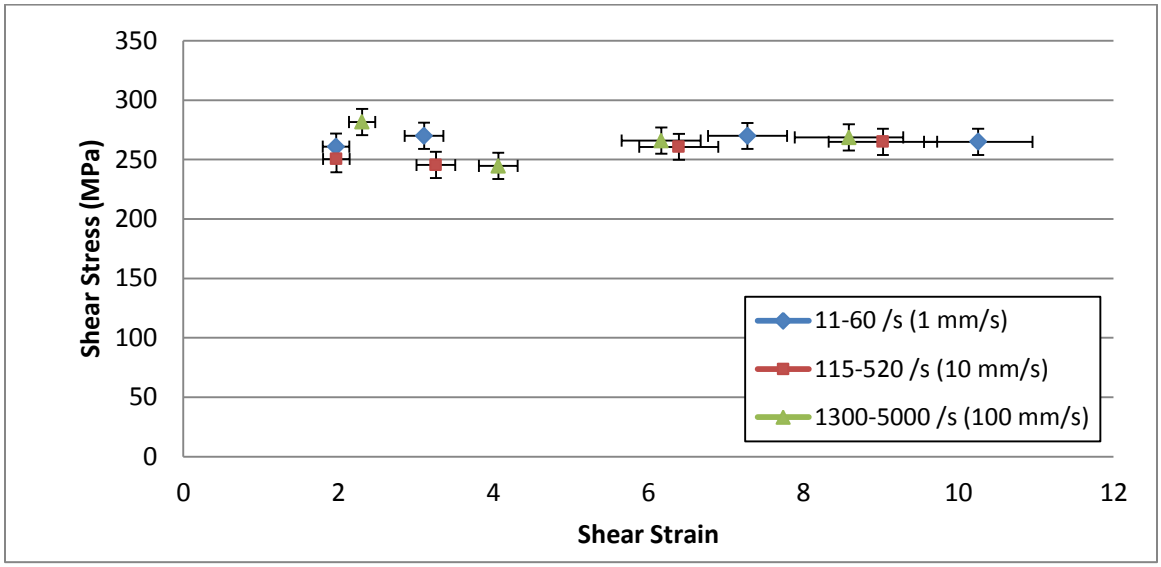

Figure 5.6: Shear Flow Stress vs. Shear Strain in hardened OFHC Cu at different strain rates (speeds), t_o=50 µm

As estimated in the previous section, the temperature of the shear plane in these trials is several hundred degrees below copper's homologous temperature of 0.5. It is clear from the figure that there is negligible influence of strain rate on the flow stress over the shear strain range of 2-10. The strain rates at each of these conditions may be inferred approximately from extrapolating the PIV data from zinc as varying between 10 to 5000/s for V_o between 1 and 100 mm/s. In estimating this strain rate range, it is assumed that the deformation zone thickness in copper and zinc is comparable, the strain rate

varies linearly with V_o, and the differences in strain imposed in the copper and zinc are accounted for. These strain rates are in good agreement with PIV measurements made directly in copper by Guo [9].

In summary, the data taken as a whole indicate that the flow stress is independent of strain and strain rate at the large strains typical of machining and at temperatures significantly lower than 0.5 T_m. Hence, it may be appropriate to use a constant value for the flow stress as input for workpiece properties in machining models, and in modeling (or interpreting) material behavior in large-strain deformation of metals.

5.6 Hardness Measurements

Vickers indentation hardness measurements were performed on the initial materials as well as the chips resulting from the cutting experiments. Four indentations were made on each chip from each α setting to characterize the hardness in each cut condition for all materials. The average hardness for each α value is recorded below in Table 5.4.

Table 5.4: Vickers Hardness. Loads designated with the material

		Zinc (10g)	Iron (25g)	Hard Cu (50g)	Annealed Cu (50g)
Error		.37	4.5	1.3	1.4
Initial HV (kg/mm^2)		41	150	121	83
α	30°	39	257	150	161
	20°	38	284	162	162
	10°	39	310	170	155
	0°	38		172	162

It is seen from these data that with the exception of zinc, all of the other metals show substantial hardness increase upon cutting, similar to what has been observed in prior

studies [6]. The lack of hardness change in zinc is likely due to its recrystallizing at room temperature between the time of the hardness measurement and the creation of the chip samples.

5.5.1 Hardness to Flow Stress Ratio

In microcrystalline metals, there exists a proportional relation between the hardness and flow stress [29]. This proportionality constant is usually taken as 3; that is by dividing the Vickers hardness by 3, the uniaxial yield stress of the metal is obtained in a consistent system of units. This relation was derived for a rigid-perfectly plastic metal so that the flow stress used is that corresponding to the highly work-hardened state, as a material in a highly-worked condition approximates a rigid-perfectly plastic metal. This ratio of hardness to flow stress was examined for the pre-hardened and annealed copper, using the flow stress data taken from machining and hardness values of the resulting chips. Prior to considering the ratio, the shear flow stress from cutting is converted to an effective (or uniaxial) flow stress using Eq. 11.

Table 5.5 Hardness to Flow stress ratios

	Hardened Cu				Annealed Cu			
α (°)	ε	σ (MPa)	HV (kg/mm²)	Ratio	ε	σ (MPa)	HV (kg/mm²)	Ratio
Precut		317	121	3.74		275	85	3.03
30°	1.1	434	150	3.39	1.9	461	161	3.43
20°	1.9	425	162	3.74	4.0	516	162	3.08
10°	3.7	452	170	3.69	5.0	503	155	3.02
0°	5.2	459	172	3.68	6.1	522	162	3.05

Table 5.5 summarizes the hardness and effective flow stress values, and their ratio. In annealed copper, the ratio is close to 3 especially in the higher strained chip. A wider variation in the ratio is seen with the hardened copper, with the average value for this ratio being ~ 3.6. It is difficult to draw any specific (and consistent) conclusion from these ratios about the hardness-flow stress relation.

6 DISCUSSION OF METHODS

The results of the cutting experiments show promise for the use of using machining as a material property test. The methodology for obtaining the flow stress as a function of strain is straightforward, and involves only the measurement of forces, chip thickness ratios and deformation zone geometry. If PIV analysis can be carried out of high speed image sequences, then direct measurement of the strain and strain rate in the deformation zone is also feasible. However, this type of image analysis is currently feasible only at low speeds. With this as the background, some of the factors that pose difficulties or are causes of uncertainty in the flow stress and strain data will be examined in this chapter. Similarities and differences with prior experimental arrangements are also discussed. This will help demarcate limitations and errors in the proposed machining methodology.

6.1 Contrast to Prior Work

Several aspects of the methods and configuration used in the present study differ from those of prior studies made with a similar objective. First, most of the prior studies used lathe turning to approximate 2-D machining. Usually, these experiments used a metal tube with the radius much larger than the wall thickness and machined the sample at the end of the tube, on the surface perpendicular to the tube axis. In the present experiments,

a linear cutting arrangement was employed, which is better for obtaining true plane strain cutting. This linear arrangement is also better for PIV analysis of the deformation as it reduces difficulties associated with constraining chip formation occurring with a curved sample. Of course, lathe turning is a much better configuration for achieving higher speeds (> 1m/s) and, hence, greater strain rates than the present study.

The present work was limited to strain rates of ~5,000 /s in the deformation zone since the cutting speed was no greater than 100 mm/s. These strain rates are still many orders of magnitude higher than those of quasi-static tests. Prior work with lathe turning was done at higher cutting speeds of 0.5-5 m/s, resulting in 1-2 orders of magnitude higher strain rates. It is interesting, however, that strain rate effects were found to be not so significant even in the prior work [27, 28] and that flow stress saturation was observed as in the present work. Taken together, the conclusion that flow stress is relatively independent of strain and strain rate in high rate metal working may be reasonable.

6.2 Error and Limitations

This experimental approach uses some assumptions which result in limitations that must be acknowledged:

Plane strain (2-D) approximation

All measurements are made with the assumption of plane strain deformation during cutting. While the samples and cutting zone geometry were designed to promote this condition ($w > 10\ t_o$), the 2-D cutting assumption is still not always perfectly satisfied. This is especially true with ‘soft’ or annealed materials which experience large amounts

of strain in cutting with large chip thickness ratios. In such cases there can be significant out of plane flow and it is also difficult to confine this deformation even with application of a constraint to the workpiece. When plane strain cannot be ensured the forces recorded in the cutting and thrust directions cannot account for this out-of-plane material flow. This out-of-plane flow also makes accurate chip thickness measurement difficult, as the chip thickness may vary across the width and not be reflective of plane strain conditions. Simply viewing the cross section of the chip gives no guarantee of observing the characteristic (maximum) chip thickness where plane strain still occurs. For these reasons, the method currently used has difficulty when testing annealed/'soft' materials.

Shear zone (plane) and smooth homogeneous flow assumption

Perhaps a fundamental limitation of this test arises from the assumptions of the shear plane (zone) model of chip formation and homogeneous (smooth) plastic flow during chip formation. It has recently been observed by Yeung [36, 37] that chip formation in cutting of a truly annealed metal (e.g., annealed copper) does not occur by the conventional shear zone idealization with smooth laminar flow. Instead the chip forms by a sinuous flow process involving extensive folding over of the metal that has little resemblance to a true shear plane model. Under such conditions it would be wrong to infer that the shear force resolved along the "shear plane" gives a representative flow stress. There is no shear plane to speak of in this type of cutting. Another important observation from Yeung's work pertains to the preparation of a truly annealed sample for cutting. Usually, the process of specimen preparation in machining the sample after annealing leaves a work hardened sublayer on the surface. A hardened layer can also be

left behind from prior cutting tests. As a result, unless extraordinary precautions are taken it is very difficult to eliminate this layer. The work of Yeung has recently outlined a method for preparing a truly annealed sample for cutting. Even though precautions were taken in the present study to create a surface devoid of work hardened layers using prior observations of the extent of these in copper by Guo [32], these may not have been sufficient to completely eliminate these layers, given the recent observations of Yeung. Thus the data for annealed copper may not reflect a flow stress typical of the initial annealed metal state. More generally, the machining approach as discussed here is unlikely to be suitable for estimating flow stress data for annealed metals. All of the prior work [2, 4, 5] appears to have not recognized this set of problems.

The chip thickness ratios and their variance with α are summarized in Table 6.1. The largest increases in chip thickness after cutting are shown by the low chip thickness ratio values, especially in the softer materials, annealed copper and iron. The small change in zinc chips over the range of α is also shown here, where the ratio at α=30°was 0.467, and at α=0° was 0.323, the highest of all materials at both conditions. Of interest here is also the comparison of copper chip ratios at α=0°. If true annealed material is cut, a significant difference is seen between the final chip thicknesses. In the present study, annealed copper sheared to just over 10 times t_o, where hardened copper chips were measured to be about 9 times t_o. Considering Ho's work described above, it is likely that the method for removing the hardened sublayer was insufficient, and the successive cuts contained some pre-hardened material. Ho has recently demonstrated true cutting of annealed copper to exhibit thickening of ~14 times t_o, further suggesting the current 'annealed' cuts contained a portion of hardened material.

Table 6.1: Chip thickness ratios in the cutting tests. $r=t_o/t_c$

	Average Chip Thickness Ratio, r			
α (°)	Annealed Cu	Hardened Cu	Zinc	Iron
30	0.278	0.441	0.467	0.165
20	0.142	0.289	0.438	0.139
10	0.114	0.154	0.380	0.147
0	0.096	0.112	0.323	

Inhomogeneous deformation in chip formation can also arise by flow localization in the form of shear bands, segmentation etc. Some of this localization was seen when cutting zinc in the present study also (Fig 5.3 d) with smaller rake angle tools. Under such conditions, the present approach may encounter some difficulties in producing accurate flow stress data. This is because the forces will fluctuate as a consequence of the localization. At the present time, unless the localization happens at low enough frequencies, it is difficult to capture the force oscillations so that the forces can be overlaid exactly onto the shear zone area corresponding to the force.

6.2.1 Experimental Errors

A common source of error arises from the rigidity of the experimental setup. Because the measurements are conducted on small length scales (t_o ~ tens of microns), small deflections of the tool-holding system or workpiece can cause the actual t_o during cutting to be different from that set initially. This can cause an error in assessment of chip thickness ratio if the set value of t_o is used. However this error can be minimized or eliminated by directly measuring the t_o value as was done in the present study.

Another source of error arises from the measurement of t_c, the deformed chip thickness. In the present case, metallography on the chip was used to obtain this.

However, as seen from Figs. 6.1 a-d, there is some uncertainty in this chip thickness measurement due to local variations in chip thickness. This was particularly evident with the iron samples in the present study wherein flow localization could have produced the somewhat larger variations in t_c (see Fig. 6.1 d). In fact this precluded cutting tests on iron to be done with a zero rake angle tool.

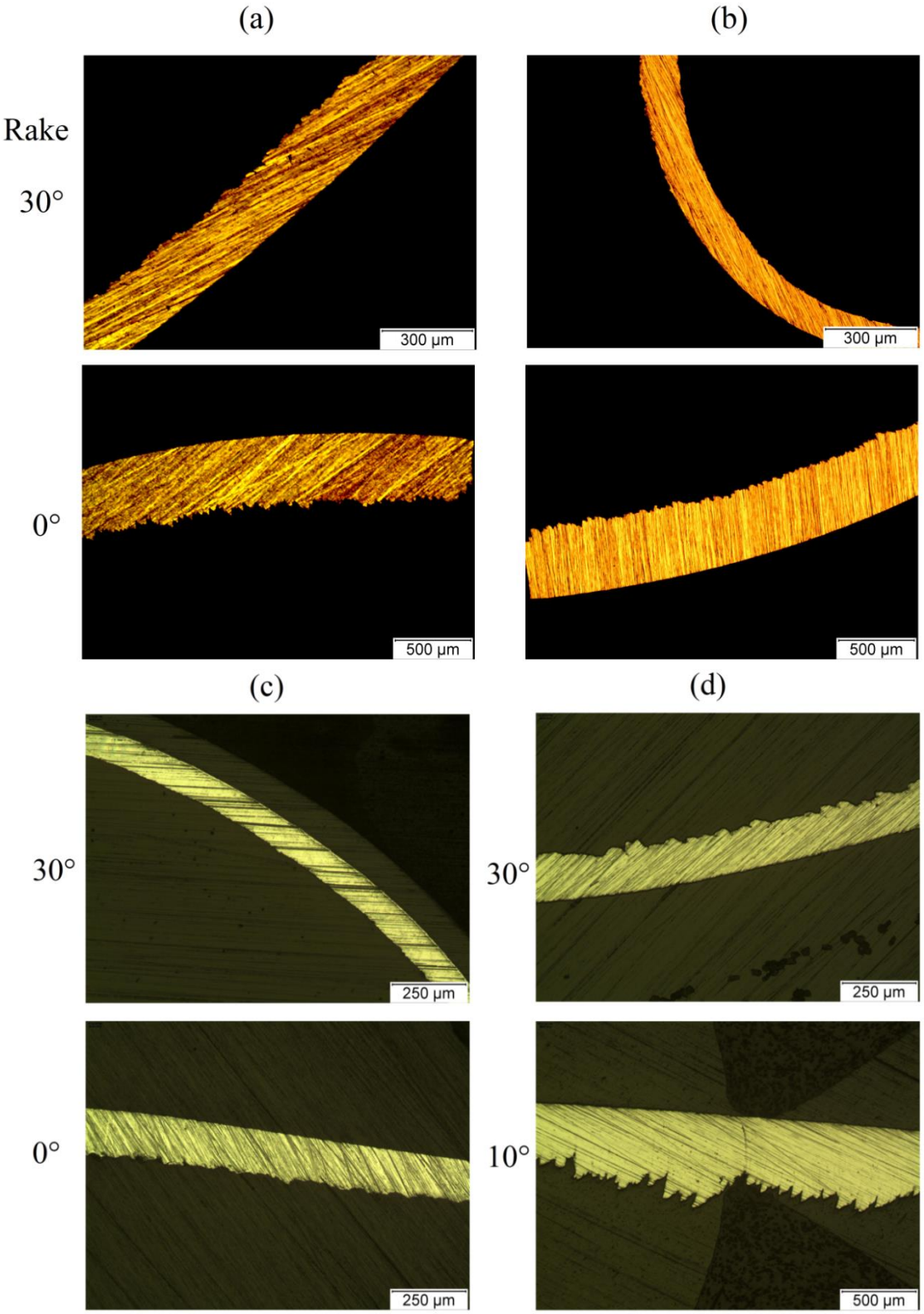

Figure 6.1: Chip thickness micrographs for chips taken from cuts at rake angles of 30° and 0° for (a) annealed copper, (b) hardened copper, (c) zinc, (d iron (30° and 10°)

To minimize this problem at least partially, care was taken to use cutting forces and chip thicknesses corresponding to the same moment of cutting to make stress and strain calculation possible. Figure 6.2 below shows one such example of the force trace and chip thickness selection. This method gave some results to visualize the material's behavior, however one can see from the shown stress and strain graphs for iron the resulting points were widely distributed and it is unlikely firm conclusions can be made from the data. This type of observed variation in chip thickness was also responsible for the lack of data at 0° rake cuts, as chips and forces from this experimental method were too irregular to be used in a meaningful calculation.

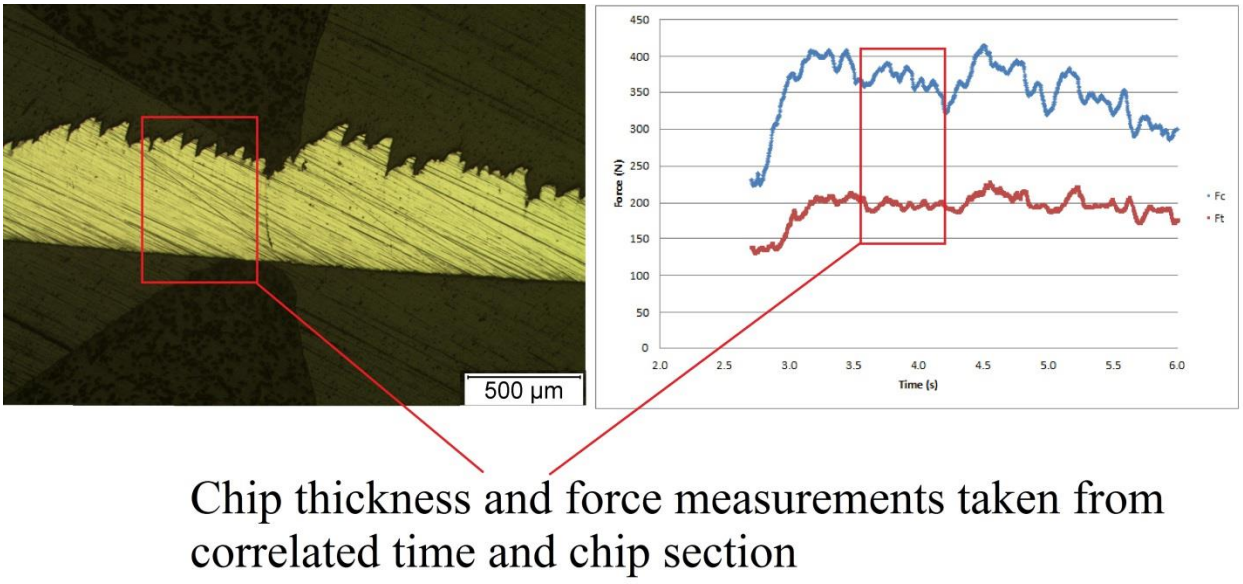

Figure 6.2: Illustration showing chip thickness and cutting force selection for iron stress-strain calculations

Using the optical microscope, it was possible to continue with calculation by ensuring the force and chip thickness data was taken at places corresponding to the same time point in the test. This method was also useful for chips in which a steady state was not seen during the whole recording, but was obtained at half-way or nearer to the end of

the force recording. Moreover, measuring the chip thickness through an optical microscope eliminates errors present when simply using a caliper or other 'maximum thickness' type measurement where only the thickest parts of the chip are measured.

An alternative approach to estimating the chip thickness ratio r, that eliminates some or all of these errors in r estimation, is by use of velocity measurements. Such measurements can be made from imaging of the deformation zone. The chip thickness ratio r can then be estimated as $r = V_c / V_o$. This however was not done in the present study.

6.2.2 Values for Measurement Error

Table 6.2 below catalogs the measurement uncertainty for the values recorded and used for calculations in the present study. These measurements include the chip geometry, cutting forces, and hardness measurements. For reference, the 2.5µm uncertainty in the measurement of t_o is 5% of the nominal value (50µm).

Table 6.2: Measurement Uncertainties by Instrument

Instrument	Measured Value	Uncertainty
Mitutoyo Height Gauge	t_o	2.5 µm
Optical Microscope	t_c	<3%
Kistler 9254 Dynamometer	F_c, F_t	<1%
Leco LM247AT Hardness Tester	HV	~1%

Compounding these measurement uncertainties into the calculated flow stresses and strain, the resulting errors are less than 5% of flow stresses and ±10% of strain magnitudes in their respective measured ranges. These were compounded through

numerical computation of each multivariate function for flow stress and strain and using the corresponding measurement uncertainties from the instruments above in Table 6.2. The resulting correlated uncertainties are tabulated for the four materials below.

Table 6.3: Error of calculated flow stress and strain. V_o=10 mm/s, t_o=50 μm

	Annealed Cu		Hardened Cu		Zinc		Iron	
α	ε	σ (MPa)	ε	σ (MPa)	ε	σ (MPa)	ε	σ (MPa)
30	0.16	20.8	0.10	19.1	0.09	17.3	0.50	39.8
20	0.32	18.2	0.14	19.1	0.09	19.1	0.36	29.4
10	0.42	17.3	0.29	19.1	0.10	17.3	0.44	29.4
0	0.51	17.3	0.40	19.1	0.13	17.3		

Another critical uncertainty is the PIV analysis as a whole, as image quality can play a large role in error due to the necessity to manually focus and illuminate the imaged area. With satisfactory images (good focus, lighting, contrast), Guo [32] has shown the present method to have measured velocity errors of less than 1% and resulting strain errors of less than 2.5% from the true value at the current cutting speeds.

7 CONCLUSIONS AND FUTURE WORK

A study has been made of the use of machining for estimating flow stress of metals at large strains and small-to-moderate strain rates (~ 10 – 10^3 /s). Data for flow stress from 3 different metals – Cu, Zn and Fe – were used as the basis for evaluating this approach. The metals encompass the common range of crystal structures and a range of flow behavior. Conclusions drawn from these tests are presented here.

Machining as a Property Test It has been shown that by appropriate control of process input parameters, V_o, t_o, and α, the deformation parameters – strain, strain rate and temperature – in chip formation can be varied over a range. This range is ~ 1-6 for effective strain, and up to 10^5/s for strain rate using velocities of ~ 2 m/s. A range of temperatures can be imposed in the deformation zone. With regard to flow stress data, these were obtained only for effective strains in the range of 1-6 and strain rates of up to ~ 1000/s in the present study. The temperature in the deformation zone with all of the metals except zinc was much less than 0.5 T_m. The use of PIV analysis on zinc cutting further supported the measurement technique here. Key assumptions in estimating the flow stress by machining are a sharp shear plane and homogeneous smooth flow of metal in chip formation. The confinement of the shear zone and homogeneity of the deformation was confirmed by experiments with zinc (with exceptions at smaller rake

angles) and prior results, both obtained using PIV characterization of the deformation. Also, PIV estimates of strain were found to be within ~0.6 of the strain value estimated from chip measurements.

Flow Stress Data The measurements showed the (dynamic) flow stress to be essentially constant and little influenced by strain or strain rate, in the effective strain range of 1-6, and strain rate range of 10-1000/s. The measured flow stresses also plateau as shear strain was varied through ranges from 2-10. The ratio of the measured flow stress in the large strain range to the flow stress at necking in tension was about 1.5 for copper versus about 4 for zinc. The unusually high ratio of dynamic flow stress to flow stress in tension recorded in zinc is likely due to the low recrystallization temperature for zinc ($0.5\ T_m = 74°C$). This proximity to the recrystallization temperature exhibits the strain rate sensitivity of zinc in comparing the flow stress in quasi-static tests and in cutting. From this behavior, the strain rate sensitivity of zinc, m, was estimated to be 0.15 in the present tests. This shows that the method may be valuable also for capturing the dynamic flow stress (without recrystallization effects) that is relevant for high-strain rate analysis.

Key sources of uncertainty in the testing have been identified. In metals wherein chip formation does not occur by a shear plane type deformation zone such as annealed copper, the proposed method may not be applicable or may yield inaccurate data. In certain metals (e.g., annealed), special care must be taken to ensure that the state of the material being cut is well-defined.

Future Work Further study is recommended to investigate the scalability of the current method to strain rates of $10^4 – 10^5$ /s more typical of high-speed machining and ballistics applications. It is important to study the saturation of flow stress and determine at what strain this occurs. This may be done using tools with large rake angles to impose strains under 1. Constrained (extrusion) machining can also be used to better control the deformation conditions during testing. Should results of these tests prove promising, machining could be confirmed as a usable large deformation materials test.

LIST OF REFERENCES

LIST OF REFERENCES

[1] D.C. Drucker. An Analysis of the Mechanics of Metal Cutting. vol. 20. Journal of Applied Physics, 1949. p.1013-1021.

[2] J.A. Williams, N. Gane. Some Observations on the Flow Stress of Metals During Metal Cutting. vol. 42. Wear: Elsevier, 1977. p.341-353.

[3] S. Kobayashi, E.G. Thomsen. Some Observations on the Shearing Process in Metal Cutting. vol. 81. Journal of Engineering for Industry: ASME, 1959. p.251-262.

[4] S. Kobayashi, R.P. Herzog, D.M. Eggleston, E.G. Thomsen. A Critical Comparison of Metal-Cutting Theories With New Experimental Data. Journal of Engineering for Industry: ASME, 1960. p.333-347.

[5] S. Ramalingam, J. Hazra. Dynamic Shear Stress - Analysis of Single Crystal Machining Studies, Journal of Engineering for Industry (1973) 939-944.

[6] T.L. Brown, S. Swaminathan, S. Chandrasekar, W.D. Compton, A.H. King, K.P. Trumble. A Low-Cost Manufacturing Process for Nano-Structured Metals and Alloys.

[7] M.E. Merchant. Basic Mechanics of the Metal Cutting Process. vol. 11. Journal of Applied Mechanics, 1944. p.168-175.

[8] M.E. Merchant. Mechanics of the Metal Cutting Process, 1. Orthogonal Cutting and a Type 2 Chip, vol. 16. Journal of Applied Physics, 1945. p.267-275.

[9] Y. Guo, M. Efe, W. Moscoso, D. Sagapuram, K.P. Trumble, S. Chandrasekar. Deformation field in large-strain extrusion machining and implications for deformation processing, Scripta Materialia 66 (2012) 235-238.

[10] M. Efe, W. Moscoso, K.P. Trumble, W.D. Compton, S. Chandrasekar. Mechanics of Large Strain Extrusion Machining and Application to Deformation Processing of Magnesium Alloys. vol. 60. Acta Materialia: Elsevier, 2012. p.2031.

[11] J.H. Weiner. vol. 77. Trans. ASME, 1955. p.1331.

[12] M.C. Shaw. Metal Cutting Principles. Oxford University Press, 1984.

[13] P.W. Bridgman. The Effect of Pressure on the Tensile Properties of Several Metals and Other Materials. vol. 24. Journal of Applied Physics: AIP Publishing, 1953. p.560-570.

[14] P.W. Bridgman. On Torsion Combined with Compression, Journal of Applied Physics 14 (1943) 273-283.

[15] U.S. Lindholm, A. Nagy, G.R. Johnson, J.M. Hoegfeldt. Large Strain, High Strain Rate Testing of Copper, Transactions of the ASME 102 (1980`) 376-381.

[16] G.R. Johnson, J.M. Hoegfeldt, U.S. Lindholm, A. Nagy. RESPONSE OF VARIOUS METALS TO LARGE TORSIONAL STRAINS OVER A LARGE RANGE OF STRAIN RATES .1. DUCTILE METALS, Journal of Engineering Materials and Technology-Transactions of the Asme 105 (1983) 42-47.

[17] W.W. Chen. Split Hopkinson (Kolsky) bar design, testing and applications, New York : Springer, New York, 2011.

[18] H. Kolsky. Stress Waves in Solids, Oxford University Press, 1953.

[19] U.S. Lindholm, L.M. Yeakley. High Strain Rate Testing: Tension and Compression. vol. 8. Experimental Mechanics, 1968. p.1-9.

[20] T. Glenn. The Origin of Strain-Rate Sensitivity in OFHC Copper. In: Bradley W, (Ed.), vol. 4. Metallurgical Transactions, 1973. p.2343-2348.

[21] G.R. Johnson, W.H. Cook. A Constitutive Model and Data for Metals Subjected to Large Strains, High Strain Rates, and High Temperatures. vol. 21. Proceedings of the 7th International Symposium on Ballistics, 1983. p.541.

[22] J.F. Alder, V.A. Phillips. The Effect of Strain Rate and Temperature on the Resistance of Aluminum, Copper, and Steel to Compression. vol. 83. Journal of the Institute of Metals, 1954. p.80.

[23] C. Zener, J.H. Hollomon. Effect of strain rate upon plastic flow of steel, Journal of Applied Physics 15 (1944) 22-32.

[24] B.T. Chao, G.H. Bisacre. The Effect of Speed and Feed on the Mechanics of Metal Cutting, Proceedings - Institution of Mechanical Engineers 165 (1951) 1-13.

[25] A.M. Freudenthal. The Inelastic Behavoir of Engineering Materials and Structures. John Wiley & Sons, Inc., 1950. p.587.

[26] W.R. Backer, E.R. Marshall, M.C. Shaw. The Size Effect in Metal Cuting. vol. 74. Transactions of the ASME, 1952. p.61-72.

[27] M.C. Shaw, I. Finnie. The Shear Stress in Metal Cutting. vol. 77. Trans. ASME, 1955. p.115-125.

[28] E.G. Thomsen, J.J.T. Lapsley, R.C. Grassi. Deformation Work Absorbed by the Workpiece During Metal Cutting. vol. 75. Trans. ASME, 1953. p.591-603.

[29] F. Lira, E.G. Thomsen. METAL CUTTING AS A PROPERTY TEST, Mechanical Engineering 89 (1967) 66-&.

[30] D. Kececioglu. Shear-Strain Rate in Metal Cutting and Its Effects on Shear-Flow Stress. vol. 80. Trans. ASME: ASME, 1958. p.158-168.

[31] D. Tabor. Hardness of Metals. Oxford Univ. Press, 1951.

[32] Y. Guo. Large Strain Surface Deformation in Machining and Sliding Processes. vol. Doctor of Philosophy: Purdue University, 2012.

[33] R.J. Adrian, J. Westerweel. Particle Image Velocimetry. vol. 30. Cambridge University Press, 2010.

[34] M. Raffel, C. Willert, S.T. Wereley, J. Kompenhans. Particle Image Velocimetry. second ed., Springer, 2007.

[35] W.F. Hosford, R.M. Caddell. Metal Forming: Mechanics and Metallurgy, Cambridge University Press, 2011.

[36] H. Yueng. Energy and Deformation in Modulation Assisted Machining. vol. Doctor of Philosophy: Purdue University, 2013.

[37] H. Yueng. In: Smith D, (Ed.), Feb. 2015.